fermentation

MDPI

Article

Valorization of the Non-Medicinal Parts of *Polygonatum sibiricum* and *Gentiana scabra* Bunge from Liaoning via Solid-State Co-Fermentation: Synergistic Antibacterial Enhancement

Chenchen Fang [1,2], Jiaqing Wang [3], Shuang Ma [1,2], Wenzhong Huang [4], Xingjiang Liu [1], Mengcan He [1], Fengchen He [1] and Junfan Fu [1,*]

[1] Majoring in Bioengineering, College of Life Engineering, Shenyang Institute of Technology, No. 1, East Section of Binhe Road, Shenfu Demonstration Zone, Fushun 113122, China; fangchen860510@126.com (C.F.); mashuang1326@126.com (S.M.); liuxibgjiang0901@163.com (X.L.); 18881098154@163.com (M.H.); hfc2501205574@foxmail.com (F.H.)

[2] Liaoning Provincial Key Laboratory of Dangerous Forest Pest Management and Control, Shenyang Institute of Technology, Shenyang 113122, China

[3] Bio-Health Industry Research Institute, Shenyang Institute of Science and Technology, No. 30, Quanyun 2nd West Road, Hunnan District, Shenyang 110167, China; jiaqing5212@163.com

[4] Fushun Agricultural and Rural Development Service Center, Building 1, Gebu East Street, Shuncheng District, Fushun 113009, China; fshwz@126.com

* Correspondence: fujunfan@163.com

Abstract

The non-medicinal parts of *Polygonatum sibiricum (P. sibiricum)* and *Gentiana scabra* (*G. scabra*) are abundant but underutilized in Liaoning Province, China, creating an environmental burden. Solid-state fermentation (SSF) offers a strategy to enhance their bioactivity, yet triple microbial co-fermentation remains underexplored. This study applied a triple microbiota—featuring *Aspergillus niger (A. niger)*, *Bacillus subtilis (B. subtilis)*, and *Saccharomyces cerevisiae (S. cerevisiae)*—to ferment the stems and leaves of both plants. Antibacterial activity against *Escherichia coli* (*E. coli*) and *Staphylococcus aureus* (*S. aureus*) was assessed via the Kirby–Bauer test, while Liquid Chromatography–Tandem Mass Spectrometry (LC–MS/MS)-based non-targeted metabolomics identified differential metabolites and enriched pathways. Co-fermentation significantly increased the inhibition zones to 17.4 ± 0.8 mm for *E. coli* and 17.7 ± 0.3 mm for *S. aureus*, a 1.8-fold improvement over the unfermented controls ($p < 0.001$). Among the 2976 metabolites detected, 1236 were differentially expressed, with Kyoto Encyclopedia of Genes and Genomes (KEGG) analysis highlighting activation of aminoacyl-tRNA biosynthesis, ABC transporter, and phenylalanine–tyrosine–tryptophan pathways. Differential abundance analysis indicated that the aminoacyl-tRNA pathway (DA score > 0.9) is critical for antimicrobial peptide synthesis. Phenylalanine derivatives, including 4-hydroxybenzaldehyde, which increased over 430-fold (Log_2 FC = 8.78), contributed to membrane-disruptive antibacterial effects. Mechanistically, *A. niger* hydrolyzes cellulose to release precursors, *B. subtilis* synthesizes antimicrobial peptides, and *S. cerevisiae* enhances metabolite solubility and excretion, collectively boosting antibacterial activity by 80%, suggesting a potent synergistic interaction among the triple microbiota. This cascade mechanism provides a scalable approach for valorizing approximately 55 million tons of traditional Chinese medicine (TCM) waste annually.

check for updates

Academic Editor: Mohammad Taherzadeh

Received: 18 September 2025
Revised: 3 November 2025
Accepted: 12 November 2025
Published: 14 November 2025

Citation: Fang, C.; Wang, J.; Ma, S.; Huang, W.; Liu, X.; He, M.; He, F.; Fu, J. Valorization of the Non-Medicinal Parts of *Polygonatum sibiricum* and *Gentiana scabra* Bunge from Liaoning via Solid-State Co-Fermentation: Synergistic Antibacterial Enhancement. *Fermentation* **2025**, *11*, 643. https://doi.org/10.3390/fermentation11110643

Copyright: © 2025 by the authors. Licensee MDPI, Basel, Switzerland. This article is an open access article distributed under the terms and conditions of the Creative Commons Attribution (CC BY) license (https://creativecommons.org/licenses/by/4.0/).

Keywords: *Polygonatum sibiricum*; *Gentiana scabra* Bunge; solid-state fermentation; non-medicinal parts; antimicrobial activity; resource valorization

1. Introduction

Liaoning Province, located in Northeast China, is a key production area for medicinal materials and is the core cultivation region for *P. sibiricum* and *G. scabra*. The total area devoted to the cultivation of Chinese medicinal materials in this province exceeds 100,000 hectares, with an annual output value of CNY 4.56 billion. The annual fresh yield of *P. sibiricum* is 37,000 tons, while *G. scabra* accounts for the largest planting area and dominates the national market, with an 82% share. However, during harvesting and processing, over 30% of the biomass, primarily non-medicinal parts such as stems and leaves, is discarded, Critically, their harvest seasons coincide, leading to the concurrent generation of substantial residues in Liaoning. Furthermore, the annual solid waste from national TCM processing exceeds 55 million tons [1–5]. This context makes a combined valorization strategy for these co-generated resources highly strategic.

Studies have demonstrated that these non-medicinal parts contain active compounds, such as phenolic acids and flavonoids, at levels comparable to those in the parts used for medicinal purposes [6,7]. Despite this, their development and utilization remain limited due to low bioavailability and recalcitrant structure [8]. Conventional disposal methods, such as incineration or landfilling, exacerbate environmental pressures [9], while chemical extraction methods suffer from low yields and high energy consumption [10].

In recent years, microbial fermentation has emerged as a promising approach to enhance the extraction of bioactive compounds from plant residues and increase resource value [11]. This process relies on the action of microbial enzymes, which efficiently degrade the plant cell wall and matrix structure. Such enzymatic hydrolysis not only facilitates the release of bound bioactive components but also promotes their biotransformation into more active or bioaccessible forms, ultimately improving both extraction yield and biological efficacy [12,13].

Furthermore, fermentation can significantly enhance the abundance of specific antimicrobial metabolites, such as phenolics (e.g., 4-hydroxybenzaldehyde) and flavonoids, which are known to exert antibacterial effects by disrupting microbial membrane integrity [14,15]. The conceptual alignment of these mechanisms with a multi-strain fermentation strategy underscores the potential of solid-state fermentation (SSF) to unlock the antibacterial value of TCM waste, forming the fundamental rationale for the triple-microbiota approach investigated in this study.

SSF technology efficiently degrades lignocellulosic agricultural residues through the synergistic action of microorganisms, converting them into high-value-added products, and has become a pivotal method for biomass resource utilization [16]. It has demonstrated significant potential in releasing and transforming bioactive components from plant substrates. For instance, Izabal Carvajal et al. showed that the co-fermentation of pomegranate peels with *A. niger* and *S. cerevisiae* effectively converted initial polyphenols into ellagic acid, a derivative with higher bioavailability and biological activity, enhancing the application value of pomegranate [17]. Similarly, SSF of soybean meal with *B. subtilis* significantly increased crude protein, soluble protein, total phenols, and flavonoid content, while reducing trypsin inhibitors [18]. Yang et al. demonstrated that fermentation of liquor distillation waste residues rich in melanoidins using *Aspergillus awamori* degraded 73.5% of melanoidins and simultaneously increased the phenolic compound and water-soluble protein contents by 52.5% and 46.5%, respectively, achieving high-value transformation

of waste [19]. The application of microbial fermentation to Chinese herbal residues is a highly promising strategy. Microorganisms can effectively degrade plant cell walls through the production of cellulases, lignases, and other enzymes, overcoming the barriers of traditional extraction. This process not only promotes the release and transformation of active ingredients, increasing yield and bioavailability, but also reduces raw material toxicity and generates novel bioactive compounds. Consequently, microbial fermentation is a sustainable and efficient approach for the valorization and green utilization of TCM waste [20].

The non-medicinal parts of *P. sibiricum* and *G. scabra* were selected as a mixed fermentation substrate based on three scientific and practical rationales: First, as both are core genuine medicinal materials in Liaoning Province, their non-medicinal parts are often co-generated as mixed waste during processing, making their combined valorization a realistic approach that aligns with industrial application scenarios [5]. Second, they exhibit complementary chemical compositions that suggest potential for synergy, whereby the polysaccharides and free amino acids from *P. sibiricum* provide essential carbon and nitrogen sources for microbial growth [2], while the characteristic aromatic compounds (e.g., iridoids and phenolic acids) of *G. scabra* can serve as direct precursors for the synthesis of antimicrobial metabolites [3,17]. Third, the mixture is expected to provide a more balanced nutritional profile (e.g., C/N ratio) for the solid-state fermentation process, helping to mitigate the risk of nutritional imbalance from a single substrate, thereby promoting inter-strain synergy and improving the overall efficiency of bioactive compound transformation [13,16].

Most studies have focused on single- or dual-bacterial systems, overlooking the potential of a triple microbiota approach. *A. niger* secretes β-glucosidase, efficiently hydrolyzing cellulose [21], while *B. subtilis* produces antibacterial lipopeptides, including surfactants [22]. *S. cerevisiae* completes the synergy by rapidly consuming soluble sugars through ethanol fermentation, supplying ethanol as an auxiliary solvent. Notably, this process involves metabolic reprogramming with up-regulation of glycolysis and fatty acid degradation and down-regulation of oxidative phosphorylation [23]. LC–MS/MS non-targeted metabolomics has confirmed that the triple-microbiota strategy can lead to the release of novel antibacterial compounds, a phenomenon yet to be explored in TCM research.

In this study, for the first time, a triple microbiota comprising *A. niger*, *B. subtilis*, and *S. cerevisiae* was applied for SSF of the non-medicinal parts of *P. sibiricum* and *G. scabra* from Liaoning Province, with the objectives of (1) identifying key antibacterial metabolites via non-targeted metabolomics; (2) evaluating the antibacterial efficacy of this fermentation system on the non-medicinal parts of these TCMs; (3) elucidating the metabolic pathway mechanisms underlying the enhancement of biological activity; and (4) establishing a resource valorization framework for the recycling and utilization of TCM processing waste, facilitating the development of an industrial-scale circular economy model.

2. Materials and Methods

2.1. Test Materials

This study did not involve animal or human subjects. The *P. sibiricum* and *G. scabra* specimens used in the experiments were collected from Hongtoushan Town, Qingyuan Manchu Autonomous County, Fushun City, Liaoning Province, in September 2024.

The inoculation strains for SSF included *A. niger* (CICC 40374), *B. subtilis* (CICC 21095), and *S. cerevisiae* (CICC 1421). The antibacterial test strains were *E. coli* (CICC 23657), purchased from the China Center of Industrial Culture Collection (CICC, Beijing, China), and *S. aureus* (CMCC (B) 26003), obtained from the National Center for Medical Culture Collections (CMCC, Beijing, China).

The sources of the main chemicals and reagents utilized in this study are as follows: Pectinase (activity: 500 U/mg) and cellulase (activity: 10,000 U/mg) were obtained from Solarbio Life Sciences Co., Ltd. (Beijing, China). Tryptone (Cat# Y008B), yeast extract (Cat# Y017A), agar (Cat# Y035C), bran (Cat# Y055), and peptone (Cat# Y001L) were supplied by Beijing Hongrun Baoshun Technology Co., Ltd. (Beijing, China). Ciprofloxacin (CAS: 85721–33–1), DMSO (CAS: 67–68–5), and vancomycin (CAS: 1404–90–6) were purchased from Macklin Biochemical Co., Ltd. (Shanghai, China). A Gram staining kit was acquired from Beckman Biotechnology Co., Ltd. (Beijing, China). Glucose, sodium chloride, and all other chemicals of analytical grade were procured from Sinopharm Chemical Reagent Co., Ltd. (Shanghai, China).

2.2. Test Processes

The overall process of each stage of the experiment is shown in Figure 1.

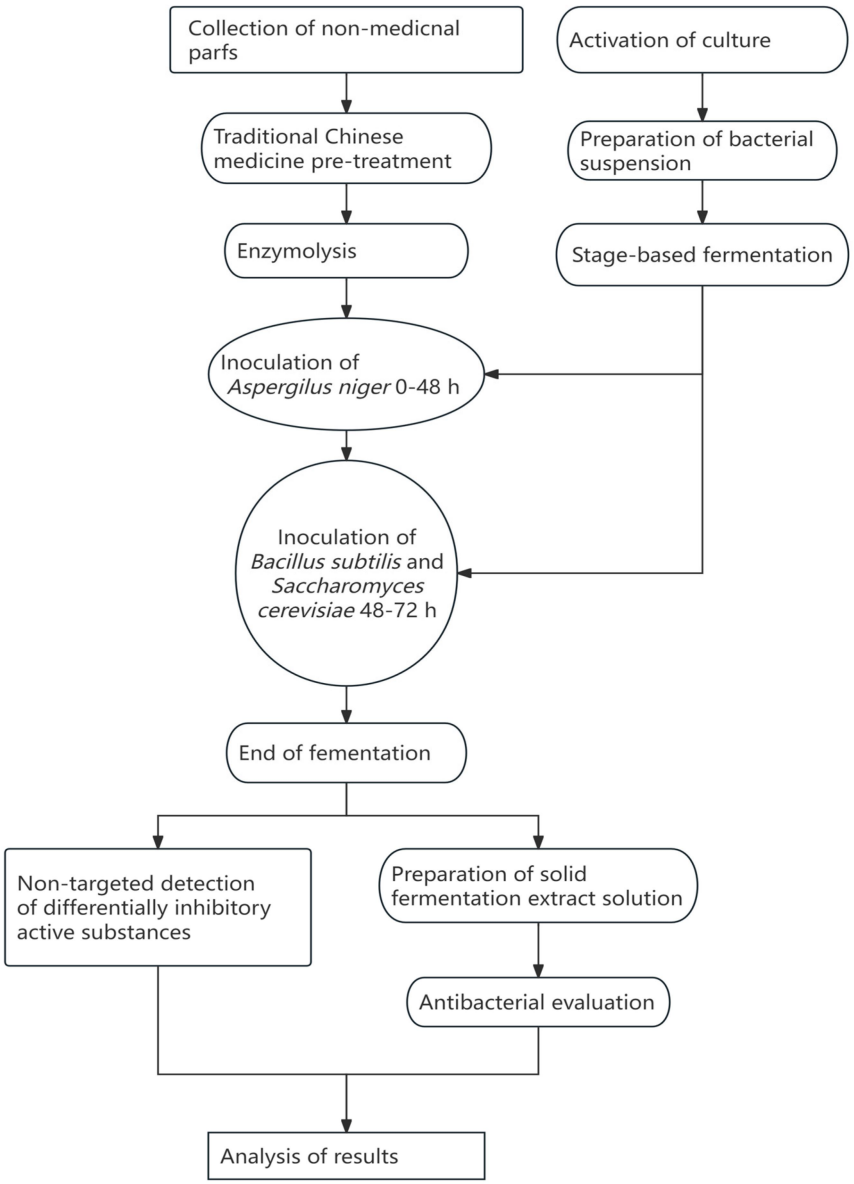


Figure 1. Schematic diagram of the triple-microbiota SSF process for valorizing non-medicinal parts (stems and leaves) of *P. sibiricum* and *G. scabra*.

2.2.1. Pre-Treatment and Fermentation of TCMs

Steps: The stems and leaves of *P. sibiricum* and *G. scabra* were washed separately, air-dried at room temperature, and then crushed (Model: JP-100A-2, Yongkang Jiupin Industry & Trade Co., Ltd., Yongkang, China) and passed through a 40-mesh sieve. The two materials were combined in a 1:1 mass ratio, with a total resulting mass of 30 g per experimental group weighed using an electronic balance (Model:LC-BX, Shanghai Lichen Bangxi Instrument Technology Co., Ltd., Shanghai, China). Distilled water was added to adjust the moisture content to approximately 45% (on a dry-weight basis) [24]. Following the addition of pectinase (1% w/w) and cellulase (1% w/w), the pH was adjusted to 4.5–5.0 for enzymatic hydrolysis conducted at 50 °C in a constant-temperature water bath (Model:HH-4, Henan Zhicheng Technology Development Co., Ltd., Gongyi, China) for 2 h [25–27]. After thorough mixing, the substrate was transferred into a conical flask, the mouth of which was sealed with a cotton stopper and kraft paper, and sterilized in an autoclave (Model: LS-75HD, Jiangyin Binjiang Medical Equipment Co., Ltd., Jiangyin, China) at 121 °C for 30 min. Following sterilization, the substrate was cooled to room temperature and stored at −4 °C until further use [28].

2.2.2. Strain Activation and Preparation of Bacterial Suspensions

All media used in this section were sterilized by autoclaving them at 121 °C for 20 min prior to use, unless otherwise specified.

(1) *A. niger* activation

Potato dextrose agar (PDA) medium was prepared by mixing an infusion obtained from 200 g of boiled peeled potatoes, 20 g of glucose, 15 g of agar, and distilled water to a final volume of 1 L. After cooling, the medium was poured into sterile Petri plates under aseptic conditions using a laminar-flow hood (Model BCM-1000, Beijing Huayi Xingchuang Technology Co., Ltd., Beijing, China). After inoculation, the PDA plates were inverted and incubated in the constant-temperature incubator (Model: DHP-9052, Shanghai Shenjia Instrument Equipment Co., Ltd., Shanghai, China) at 28 °C for 2–3 days until black and fluffy colonies appeared.

(2) *B. subtilis* activation

Luria–Bertani (LB) liquid medium was prepared by mixing 10 g of tryptone, 5 g of yeast extract, 10 g of NaCl, and distilled water up to a volume of 1 L; the pH was then adjusted to pH 7.0. After inoculation, the medium was incubated at 37 °C on the shaker (Model: TS-110X90, Chuhengyi, Hangzhou, China) at 180 rpm for 24 h. Gram staining and microscopic (Model: MSD100-9, Murzider, Shenzhen, China) examination were performed to confirm bacterial morphology.

(3) *S. cerevisiae* activation

Yeast Extract–Peptone–Dextrose (YPD) medium was prepared by mixing 10 g of yeast extract, 20 g of peptone, 20 g of glucose, and distilled water up to a volume of 1 L, and the pH was adjusted to 6.0. to standardize the initial growth conditions for the *S. cerevisiae* and ensure batch-to-batch consistency. Following inoculation, the medium was incubated at 30 °C on a shaker at 180 rpm for 24 h. Microscope observation confirmed the presence of oval yeast cells.

(4) Preparation of bacterial suspensions

(i) *A. niger* spore suspensions: Five milliliters of sterile water was added to the activated *A. niger* plate. Using an inoculation loop, spores were gently scraped to form a homogeneous suspension. The spore concentration was

determined using a hemocytometer and adjusted to 1×10^6 CFU/g of the medicinal substrate.

(ii) Suspensions of *B. subtilis* and *S. cerevisiae*: The activated bacterial or yeast cultures were centrifuged (Model:TDZ5-WS, Beijing Jiahui Centrifuge Co., Ltd., Beijing, China) at 4000 rpm for 10 min. The supernatant was discarded, and the cells were resuspended in sterile water. The optical density (Model: UV-5500PC, Shanghai Youke Instrument Co., Ltd., Shanghai, China) at 600 nm (OD_{600}) was measured using a spectrophotometer and adjusted to 1.0 to standardize the cell concentration.

2.2.3. Stage-by-Stage Fermentation

The fermentation substrate consisted of a mixed material containing 40% stems and leaves of *P. sibiricum*, 40% stems and leaves of *G. scabra*, and 20% bran. The bran was added as a bulking agent to enhance substrate porosity and aeration and provide auxiliary nutrients for the fermenting microorganisms [29]. The substrate was inoculated with *A. niger* at 1×10^6 CFU/g, *B. subtilis* at 5×10^5 CFU/g, and *S. cerevisiae* at 2×10^6 CFU/g following pre-treatment, with a fixed inoculation volume of 15%. The liquid-to-solid ratios were 0.13:1, 0.009:1, and 0.009:1 (mL:g) for *A. niger*, *B. subtilis*, and *S. cerevisiae*, respectively. The total fermentation period spanned 72 h and comprised two stages. The first was a 48-h *A. niger* monoculture in a shaker (28 °C, 100 rpm, pH 5.5). Substrate moisture was maintained at 65% via sterile water supplementation, as determined via gravimetric monitoring. To ensure adequate oxygen supply, the substrate was turned over every 12 h aseptically in a laminar flow hood. The second stage (48–72 h) began with the co-inoculation of *B. subtilis* and *S. cerevisiae*, after which the culture was transferred to a static incubator at 30 °C. Sterile gauze covered the container throughout the process [30,31].

For the control groups (Control-1d and Control-3d), the same substrate preparation and sterilization procedures were applied. These control substrates were incubated under identical conditions but without the inoculation of any microorganisms. Control-1d samples were collected immediately after sterilization, while Control-3d samples were collected after 3 days of incubation.

2.2.4. Preparation of Solid Fermentation Extract Solution

The product obtained from solid fermentation was mixed with sterile water in a ratio of 1:20 (g/mL). The sample was then extracted at 40 °C using an ultrasonic cell disruption instrument (Model: KH-500DB, Kunshan Hechuang Ultrasonic Instrument Co., Ltd., Kunshan, China) at a power of 160 W for 1 h. This ultrasonic power was selected in accordance with the established principle that controlled energy input is crucial to prevent the thermal degradation of thermolabile bioactive compounds during ultrasound-assisted extraction [32]. After extraction, the mixture was centrifuged at 4000 rpm for 10 min, and the supernatant was collected for further analysis.

2.2.5. Antibacterial Evaluation

Antibacterial activity was assessed against *E. coli* (Gram-negative) and *S. aureus* (Gram-positive) using the filter paper disk method [33,34], two strains that were selected as representative model organisms due to their distinct cell wall structures, which provide a fundamental basis for assessing activity against major bacterial classes [35]. Nutrient agar (NA) medium was melted and poured into Petri dishes under aseptic conditions and allowed to solidify. An aseptic cotton swab was dipped into *E. coli* and *S. aureus* bacterial suspensions (1×10^8 CFU/g) and evenly spread across the surface of the solidified NA medium, with excess liquid absorbed. Sterilized filter paper disks (6 mm in diameter) were then placed on the medium using aseptic forceps. For the experimental group, 10 μL of

the test sample was applied to each disk. The positive control (AC) group used 15 μg/mL Ciprofloxacin for *E. coli* and 15 μg/mL Vancomycin for *S. aureus*, while the negative control (NC) employed 10% DMSO. The culture dishes were incubated at 37 °C for 24 h in a horizontal position. The diameter of the inhibition zones was measured with a vernier caliper accurate to 0.1 mm. Each experiment was independently repeated three times to evaluate the inhibitory effects of the samples on the target bacteria. All measurements of inhibition zone diameters are presented as means ± standard deviation (SD).

2.2.6. Detection of Non-Targeted Differential Antibacterial Active Substances

(1) Sample groups and preparation

Non-targeted metabolomic analysis was performed on samples from three distinct groups: Control-1d, the sterilized and unfermented plant substrate serving as the metabolic baseline; Control-3d, the sterilized substrate incubated for 3 days without inoculation to account for changes from incubation conditions; and Mic3-E1-3d, the experimental group subjected to the 3-day staged co-fermentation with the triple microbiota (*A. niger*, *B. subtilis, and S. cerevisiae*), as described in [Section 2.2.3].

(2) Sample extraction

All sample replicates were stored at −80 °C until analysis. For extraction, the frozen samples were thawed on ice and then ground thoroughly in liquid nitrogen, and 20 mg (±1 mg) of each sample was weighed and placed into correspondingly numbered centrifuge tubes. Subsequently, 400 μL of a 70% methanol–water internal standard extraction solution was added, followed by shaking at 1500 rpm for 5 min, and the mixture was left to stand on ice for 15 min. The samples were then centrifuged at 12,000 rpm for 10 min at 4 °C. Next, 300 μL of the supernatant was transferred to another numbered centrifuge tube and stored at −20 °C for 30 min. Afterward, centrifugation at 12,000 rpm was performed at 4 °C for 3 min, and 200 μL of the resulting supernatant was transferred into the inner tube of the corresponding sample vial for on-machine analysis. This procedure was carried out by Shenggong Biotechnology Engineering (Shanghai, China) Co., Ltd.

(3) LC–MS/MS analysis

High-performance liquid chromatography coupled with tandem mass spectrometry (LC–MS/MS) was employed for substance identification [36,37]. Chromatographic separation was performed using a Waters ACQUITY Premier HSS T3 column (1.8 μm, 2.1 mm × 100 mm). The mobile phase A consisted of water containing 0.1% formic acid, and mobile phase B consisted of acetonitrile containing 0.1% formic acid. The column temperature was maintained at 40 °C, with a flow rate of 0.4 mL/min and an injection volume of 4 μL. The elution gradient program was as follows: at 0.0 min, mobile phase A was 95% and B was 5%; at 1.0 min, A was 80% and B was 20%; at 3.0 min, A decreased to 1% and B increased to 99%, which was maintained until 4.5 min; at 4.6 min, A returned to 95% and B to 5%, and this ratio was maintained until 6.0 min.

MS analysis was conducted using specific instrument parameters. The spray voltage was set to 3500 V in positive ion mode (ESI^+) and 3200 V in negative ion mode (ESI^-). The sheath gas flow rate was 30 arb, and the auxiliary gas flow rate was 5 arb. The ion transfer tube temperature was maintained at 320 °C, and the atomization temperature at 300 °C. For MS1, the scan range was 75–1000 Da with a resolution of 35,000, an automatic gain control (AGC) target of 1.00×10^6, and a collision energy of 50 V. The MS2 scan range was also 75–1000 Da, with a resolution of 17,500, an AGC target of 2.00×10^5, and a collision voltage range of 30–40.5 V. Additional parameters included a signal intensity threshold of 1.00×10^6 cps, a candidate ion number of 10, and a dynamic exclusion time of 3 s.

(4) Data processing and statistical analysis

Data processing and statistical analysis After conversion of the raw MS data to mzML format using ProteoWizard (3.X), peak extraction, alignment, and retention time correction were performed using the XCMS (4.5.2) program. Metabolite peaks with a missing rate exceeding 50% within sample groups were filtered out. The remaining missing values were imputed using a combination of the K-nearest neighbor (KNN) algorithm and one-fifth of the minimum value method. Peak areas were subsequently corrected using Support Vector Regression (SVR). Metabolite identification was conducted by searching the laboratory's self-built database, integrated public libraries, and predictive libraries. Metabolites with a comprehensive identification score greater than 0.5 and a coefficient of variation (CV) of less than 0.3 in quality control (QC) samples were retained for subsequent analysis.

Quality control assessments confirmed high data reliability, with Pearson correlation coefficients among QC samples greater than 0.99, CV values for internal standards below 0.03, and over 85% of all metabolites exhibiting CV values less than 0.3 (Table S1, Supplementary Materials).

Multivariate statistical analyses were employed to evaluate the data. Principal component analysis (PCA) was performed using unit variance (UV) scaling, as shown in Formula (1):

$$x' = \frac{x - \mu}{\sigma} \tag{1}$$

Here, μ is the mean, and σ is the standard deviation.

Orthogonal partial least squares–discriminant analysis (OPLS-DA) was applied after $\log_2$ transformation and mean centering of the data, as shown in Formula (2):

$$x' = x - \mu \tag{2}$$

The model's validity was confirmed through 200 permutation tests. Hierarchical cluster analysis (HCA) was conducted using the R package ComplexHeatmap (version 2.9.4) with UV-scaled data.

Differential metabolites were screened based on the criteria of a variable importance in projection (VIP) value greater than 1.0 from the OPLS-DA model and a false discovery rate (FDR)-adjusted *p*-value of less than 0.05. KEGG pathway enrichment analysis was performed using a hypergeometric test, with the *p*-value calculated as Formula (3):

$$P = 1 - \sum_{i=0}^{m-1} \frac{\binom{M}{i}\binom{N-M}{n-i}}{\binom{N}{n}} \tag{3}$$

where N is the total number of metabolites with KEGG annotations, n is the number of differential metabolites in N, M is the number of metabolites in a specific pathway, and m is the number of differential metabolites in M. The Rich Factor was defined as m/M. Pathway enrichment significance was defined as an FDR value of less than 0.05. The differential abundance (DA) score was calculated to evaluate the overall perturbation direction of each KEGG pathway using the following formula: (number of up-regulated metabolites—number of down-regulated metabolites)/total number of annotated metabolites in the pathway. Here, the values ranged from −1 to 1.

Detailed information regarding software versions, analytical parameters, and computational methods is provided in Table S2 (Supplementary Materials).

3. Results

3.1. Antimicrobial Activity of Unfermented and Fermented Samples

The diameter of the inhibition zone for the NC was minimal (6.0 ± 0.2–6.0 ± 0.3 mm), essentially matching the diameter of the filter paper (6 mm) (Figure 2a,f). The positive control (AC) confirmed the sensitivity of the assay: Ciprofloxacin (15 μg/mL) produced an inhibition zone of 14.7 ± 0.4 mm against *E. coli* (Figure 2e) and Vancomycin (15 μg/mL) produced a zone of 14.3 ± 0.5 mm against *S. aureus* (Figure 2j), consistent with the M07-A10 standards of the Clinical and Laboratory Standards Institute (CLSI) [38]. The Control-1d and Control-3d samples exhibited modest antibacterial activity against both *E. coli* and *S. aureus*; however, there was no significant difference between these groups ($p > 0.05$), with inhibition zone diameters ranging from 6.2 ± 0.6 to 7.3 ± 0.4 mm (Tukey's test, $p > 0.05$; Table 1). Following SSF, the MIC3-E1-3d sample demonstrated significantly enhanced antibacterial activity compared to the control groups (ANOVA, $p < 0.001$), with inhibition zones measuring 17.4 ± 0.8 mm for *E. coli* and 17.7 ± 0.3 mm for *S. aureus*, approximately 1.8 times larger than Control-1d ($p < 0.05$) and 1.77 times larger than Control-3d ($p < 0.05$). These findings align with previous research on the antibacterial mechanisms of small-molecule phenolic compounds. Phenolic compounds, such as 4-hydroxybenzaldehyde, derived from plant or microbial metabolism, can disrupt bacterial cell membrane integrity, potentially inducing oxidative damage that increases membrane permeability, causes leakage of intracellular contents, and ultimately inhibits or kills bacteria [39]. This study suggests that SSF may produce or release a substantial amount of such active molecules, thereby significantly enhancing antibacterial efficacy.

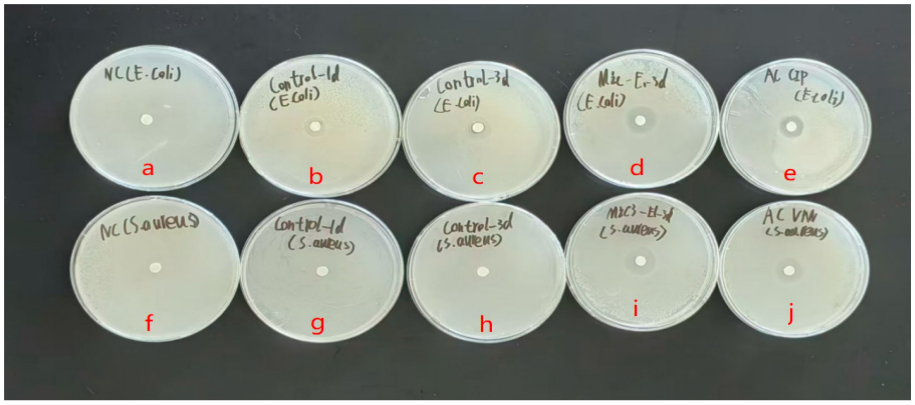


Figure 2. Antibacterial activity of the samples against *E. coli* and *S. aureus*: (**a**,**f**) negative control (NC, 10% DMSO); (**b**,**g**) unfermented substrate control (Control-1d); (**c**,**h**) incubated substrate control without inoculation (Control-3d); (**d**,**i**) solid-state co-fermentation product (Mic3-E1-3d); (**e**) positive control for *E. coli* (15 μg/mL Ciprofloxacin); (**j**) positive control for *S. aureus* (15 μg/mL Vancomycin). Scale bar = 6 mm.

Table 1. Inhibition zone diameters (mm, mean ± SD) of unfermented and co-fermented samples against *E. coli* and *S. aureus*.

Test Strain	NC	AC	Control-1d	Control-3d	Mic3-E1-3d
E. coli	6.0 ± 0.2 ***	14.7 ± 0.4 ***	6.2 ± 0.6 ***	6.6 ± 0.5 ***	17.4 ± 0.8 ***
S. aureus	6.0 ± 0.3 ***	14.3 ± 0.5 ***	6.4 ± 0.5 ***	7.3 ± 0.4 ***	17.7 ± 0.3 ***

*** $p < 0.001$ vs. all control groups; n = 3 independent replicates.

As shown in Figure 2d,i, the inhibition zones of MIC3-E1-3d surpassed those of the *E. coli* group (17.4 ± 0.8 mm) and *S. aureus* group (17.7 ± 0.3 mm), representing an 80% increase compared with the non-fermented group ($F = 36.72$, $p < 0.001$). The

inhibition zones of the positive controls (Ciprofloxacin and Vancomycin) complied with CLSI standards, confirming the reliability of the experimental system and indicating that solid co-fermentation can release potent antibacterial substances.

3.2. Non-Targeted Metabolomics Analysis of Fermented Samples

3.2.1. Metabolite Identification and Quality Control

In this study, LC–MS/MS technology was applied for the non-targeted metabolomics analysis of three sample groups—Control-1d, Control-3d, and Mic3-E1-3d—each with three replicates, resulting in a total of nine samples. A total of 2976 high-confidence metabolites were identified after rigorous quality control filtering (see Section 2.2.6 for data processing details), including 1619 detected in positive ion mode (T3_positive) and 1357 in negative ion mode (T3_negative). Secondary verification confirmed 2486 metabolites (Table 2). Quality control analysis demonstrated the high reliability of the data, with total ion current retention times and peak intensity consistency for QC samples exceeding 95% (Figure 3), Pearson correlation coefficients greater than 0.99 (Figure 4), and CV for internal standards below 0.03 (Table 3). Moreover, over 85% of the metabolites exhibited CV values below 0.3, indicating stable and reproducible measurements.

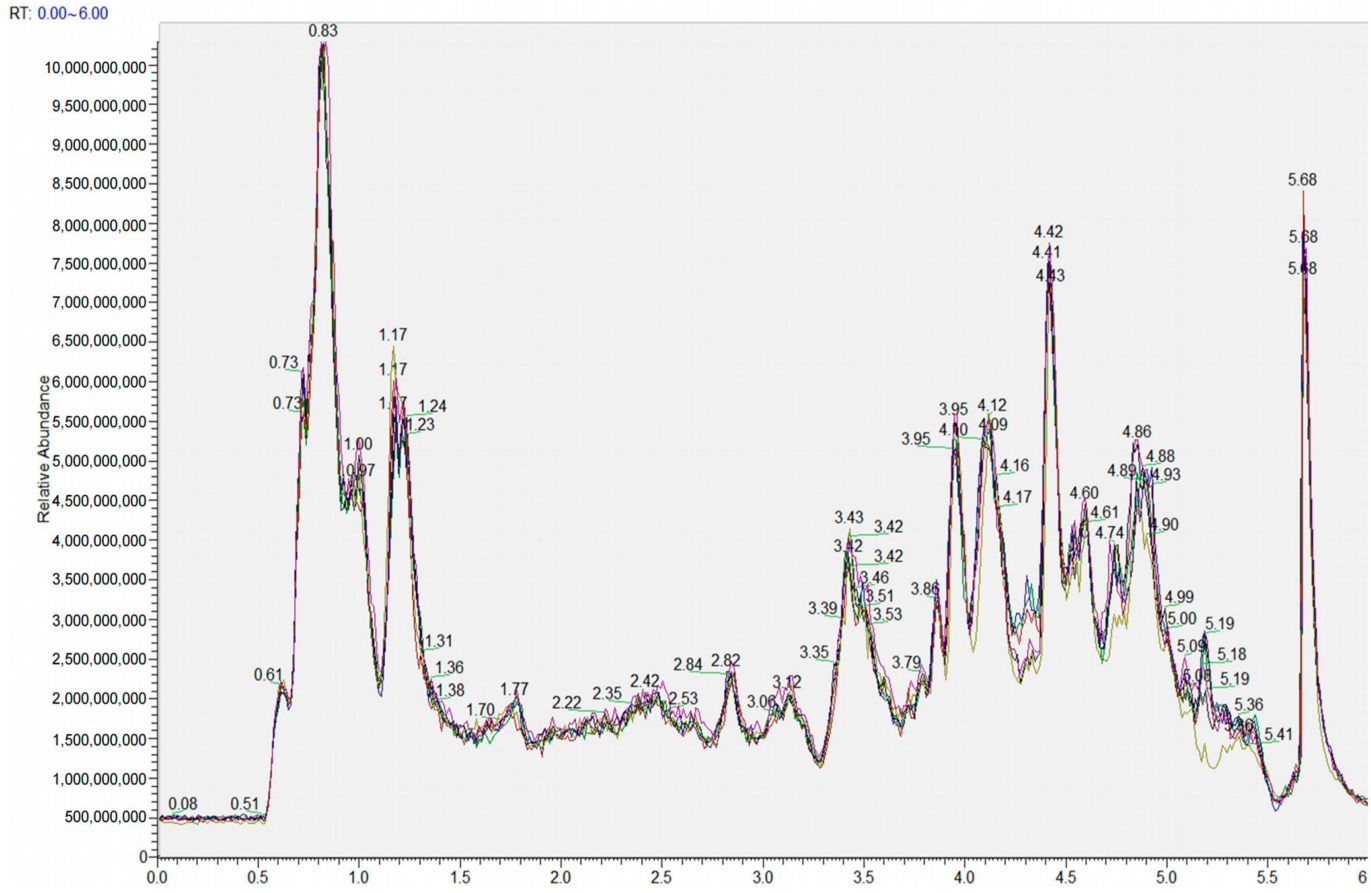


Figure 3. QC sample mass spectrum detection Total Ion Chromatogram (TIC) overlap graph. Note: This is a superimposed chromatogram of the total ion current (TIC) from the QC sample's mass spectrometry data. The results show high overlap in the TIC curves of metabolites, with consistent retention times and peak intensities, indicating good signal stability when the same sample is analyzed at different times.

Table 2. Statistical table depicting the number of metabolites identified. Note: Nine samples were selected and divided into three groups for metabolic study, and 2976 metabolites were detected.

Ion Mode	All	T3_Positive	T3_Negative
Quantity of metabolites	2976	1619	1357
Quantity of metabolites for secondary identification	2486	1254	1232

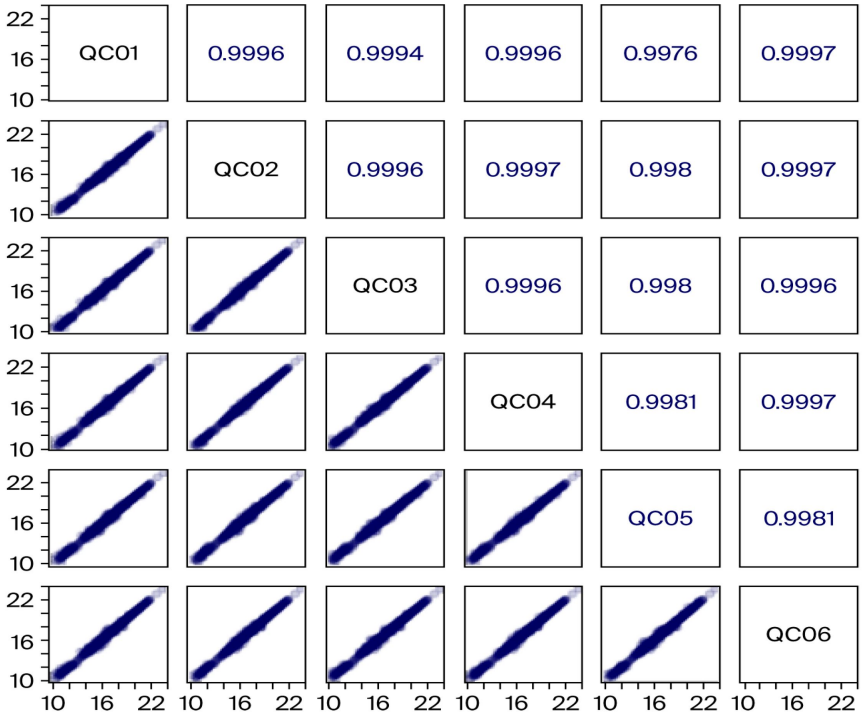


Figure 4. Pearson correlation matrix of quality control (QC) samples. The high correlation coefficients (all >0.99) among all QC replicates confirm the high reproducibility and reliability of the metabolomics data.

Table 3. Stability of internal standards in QC samples.

Index	Q1 (Da)	RT (min)	CV
MWS04428-IS-N	144.1101	4.57	0.0116
MWS4243-IS-N	198.0320	2.28	0.0189
MWS3085-IS-N	278.9911	3.78	0.0234
MWS04198-IS-N	126.1448	4.08	0.0284

3.2.2. Multivariate Statistics

The OPLS-DA score plot demonstrated that the metabolic profiles of the Control-1d, Control-3d, and Mic3-E1-3d groups were clearly distinct (Figure 5). The validity of the model was confirmed through 200 permutation tests, yielding a Q^2 value of 0.957 (>0.5, $p = 0.005$) (Figure 6). PCA further verified significant metabolic differences between groups, with robust intra-group clustering observed (Figure 7).

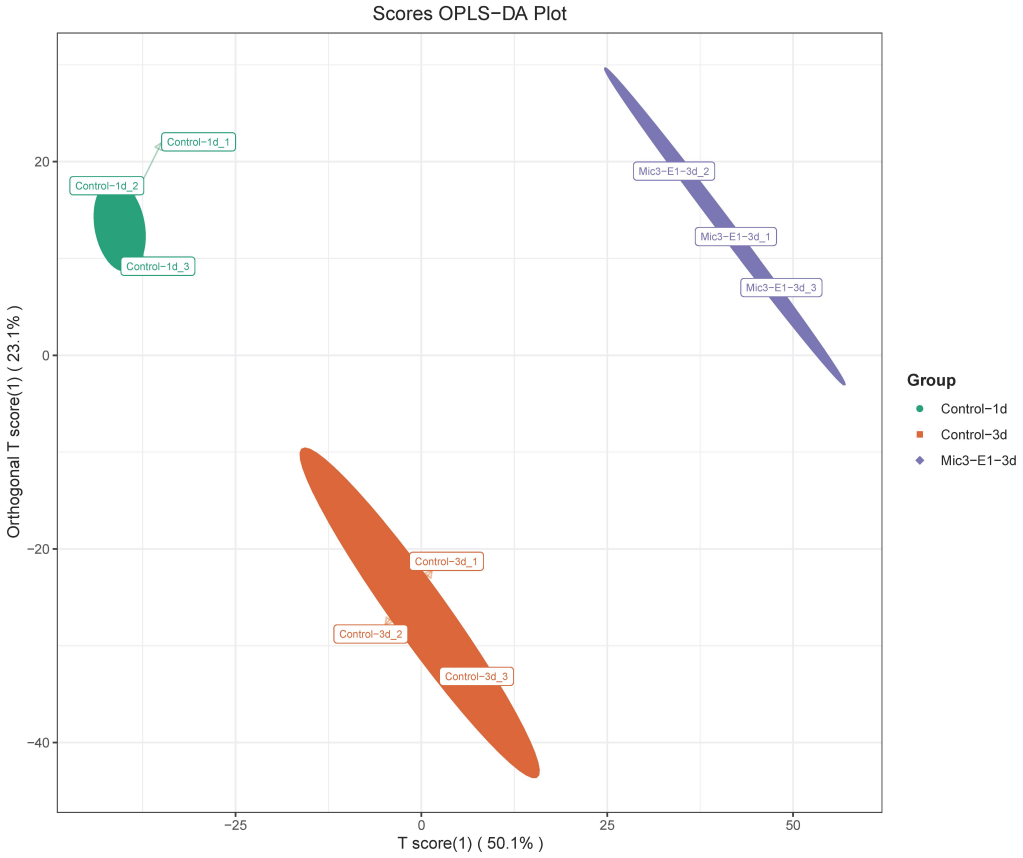


Figure 5. OPLS-DA score plot derived from the LC-MS metabolomic profiles. The model shows clear separation between the sample groups: Control-1d (unfermented baseline), Control-3d (incubated control), and Mic3-E1-3d (triple microbiota fermentation). The percentages of variance explained by the predictive component (t(1)) and the orthogonal component (to (1)) are indicated.

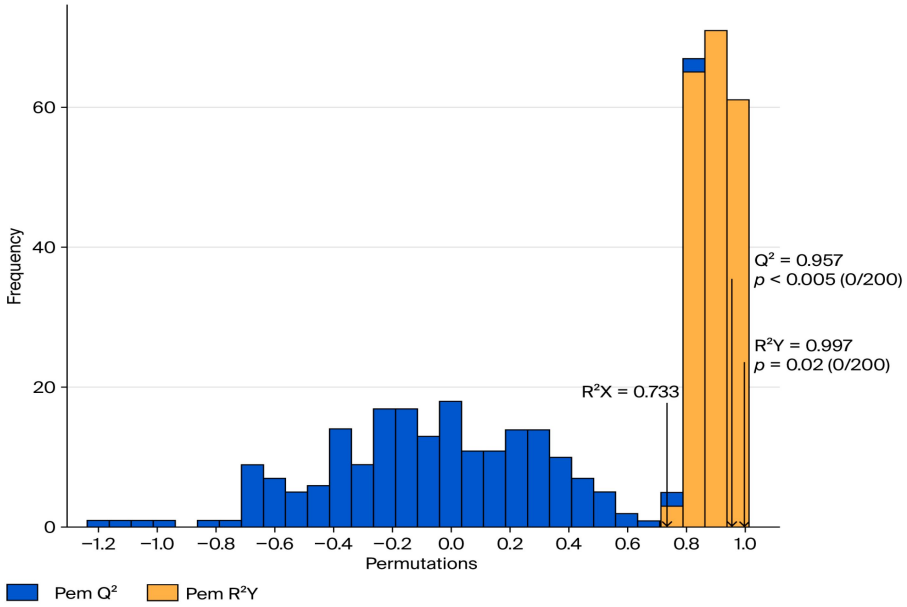


Figure 6. Permutation test results for the OPLS-DA model (200 permutations). The scatter plot shows the correlation between the correlation coefficients of the permuted models and their respective Q^2 values. The vertical dashed line indicates the position of the original model's Q^2 value (0.62). The model is considered valid and robust as the original Q^2 value is significantly higher than all permuted Q^2 values ($p < 0.05$).

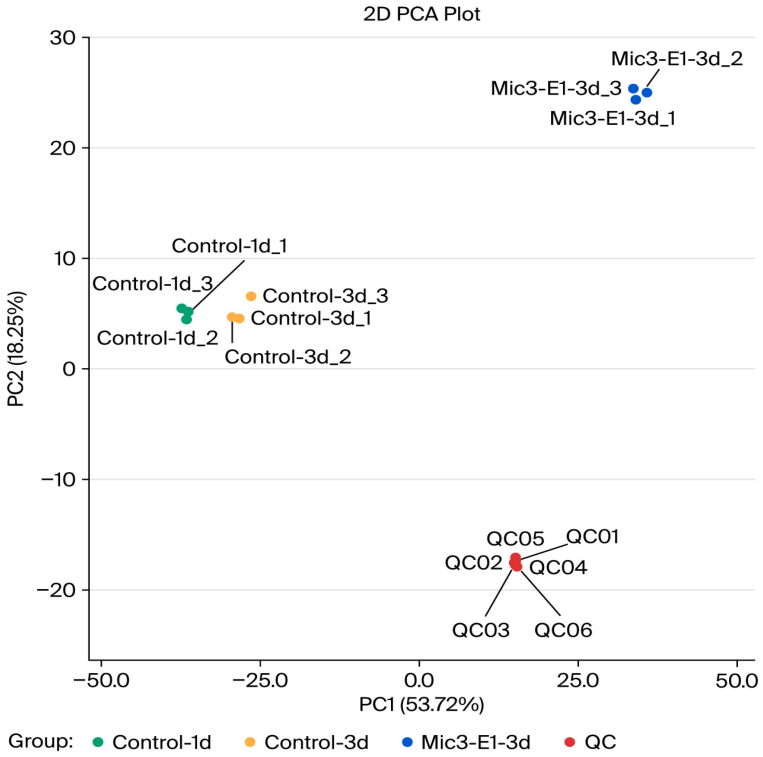


Figure 7. PCA score chart of all samples. Note: PC1 accounted for 53.72% of the variance, and the clustering trends of each group were significant.

3.2.3. Differential Metabolite Screening

Compared with Control-1d, 1236 differential metabolites were identified in Mic3-E1-3d, including 713 down-regulated and 523 up-regulated compounds. In comparison with Control-3d, 1150 differential metabolites were detected, with 599 down-regulated and 551 up-regulated (Table 4, Figure 8). Among these differential metabolites, the levels of benzene and its derivatives (e.g., benzoic acid), organic acids (e.g., acetic acid), and glycerophospholipids (e.g., phosphatidylcholine) were significantly increased. The volcano plot in Figure 8 provides an intuitive representation of the distribution of these differences. Notably, among the 20 most significantly altered metabolites in Mic3-E1-3d compared with Control-3d, key antibacterial compounds such as 1,1′-(Tetrahydro-6a-hydroxy-2,3a,5-trimethylfuro[2,3-d]-1,3-dioxole-2,5-diyl)bis-ethanone (2,3-butanedione trimer) ($Log_2FC = 9.57$) and 4-Hydroxybenzaldehyde ($Log_2FC = 8.78$) were significantly up-regulated (Figure 9a). Figure 9b (radar chart) further verifies the comprehensive differences in these top 20 metabolites: red dots represent up-regulated metabolites, green dots represent down-regulated ones, and the size of dots corresponds to VIP values (a key criterion for differential metabolite screening, VIP > 1). For example, 2,3-butanedione trimer and 4-Hydroxybenzaldehyde are presented as large red dots, confirming their high variation amplitude (Log_2FC) and strong statistical significance (high VIP values). Category enrichment analysis of key antibacterial metabolites revealed that benzene derivatives (e.g., 3,5-Dimethoxycinnamic acid and 4-Hydroxybenzaldehyde), nitrogen-containing compounds (e.g., Leu-Ile), and ketones (e.g., 2,3-butanedione trimer, which features a furan ring in its structure $Log_2FC = 9.57$) formed a synergistic cluster, highlighting the complementary metabolic mechanisms of the triple microbiota (Figure 10). Furthermore, Figure 10 shows that benzene derivatives and organic acids constitute a core synergistic cluster, with both classes displaying significant positive correlations with flavonoids and FAs.

Table 4. Statistical table concerning the number of differential metabolites.

Group Name	All Significant Differences	Down-Regulated	Up-Regulated
Mic3-E1-3d_vs_Control-1d	1236	713	523
Mic3-E1-3d_vs_Control-3d	1150	599	551

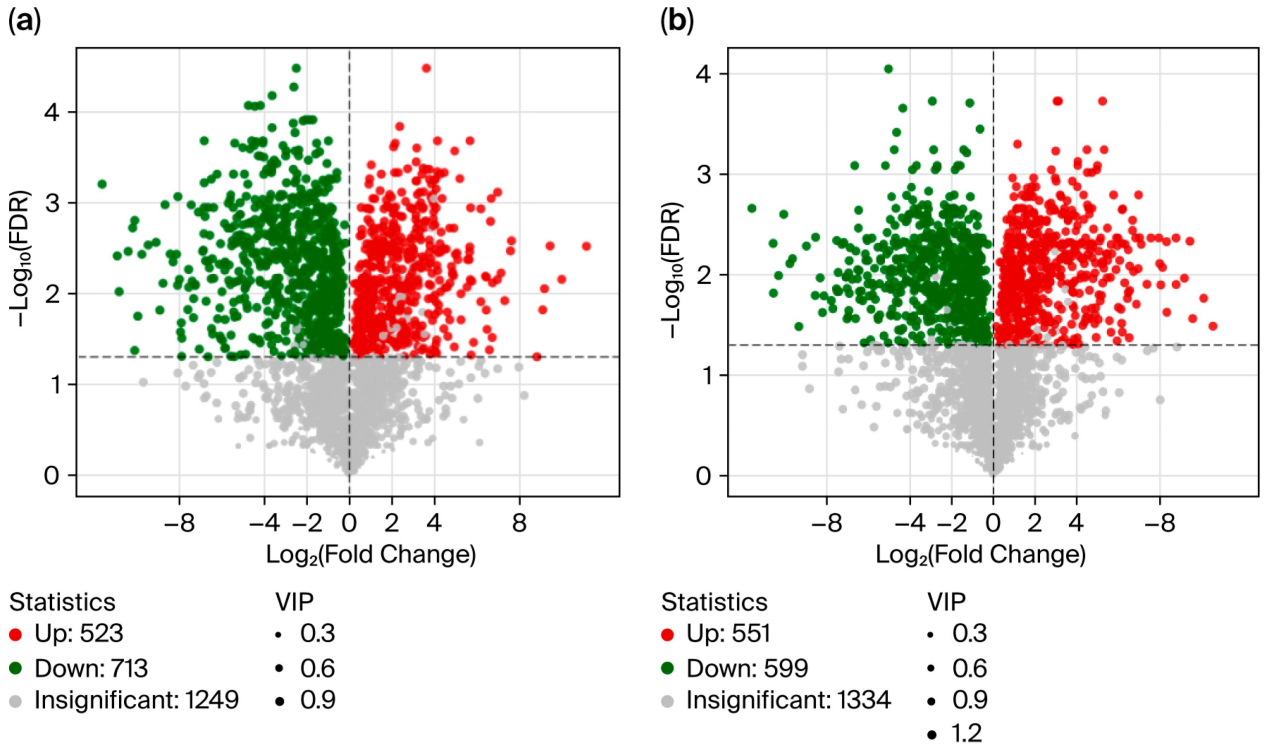
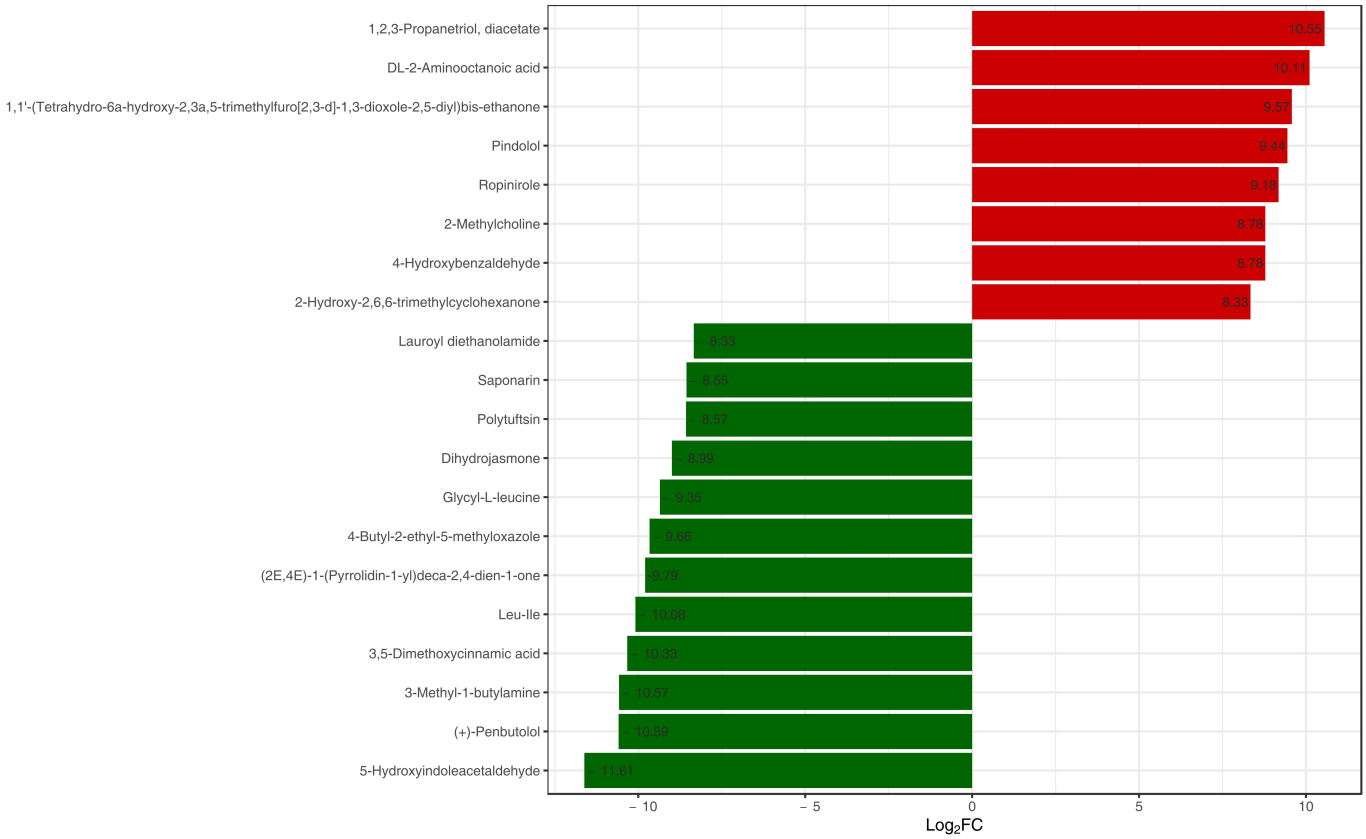


Figure 8. Volcano plots of differential metabolites. (**a**) Comparison between Mic3-E1-3d and Control-1d. (**b**) Comparison between Mic3-E1-3d and Control-3d. Metabolites are plotted based on their Log_2 fold change (*x*-axis) and statistical significance ($-Log_{10}$ FDR, *y*-axis). Dots located above the horizontal significance threshold and to the far left (down-regulated) or far right (up-regulated) of the vertical fold change thresholds represent statistically significant differential metabolites. The exact numbers of up-regulated, down-regulated, and non-significant metabolites are provided in the figure.

3.2.4. Metabolic Pathway Enrichment

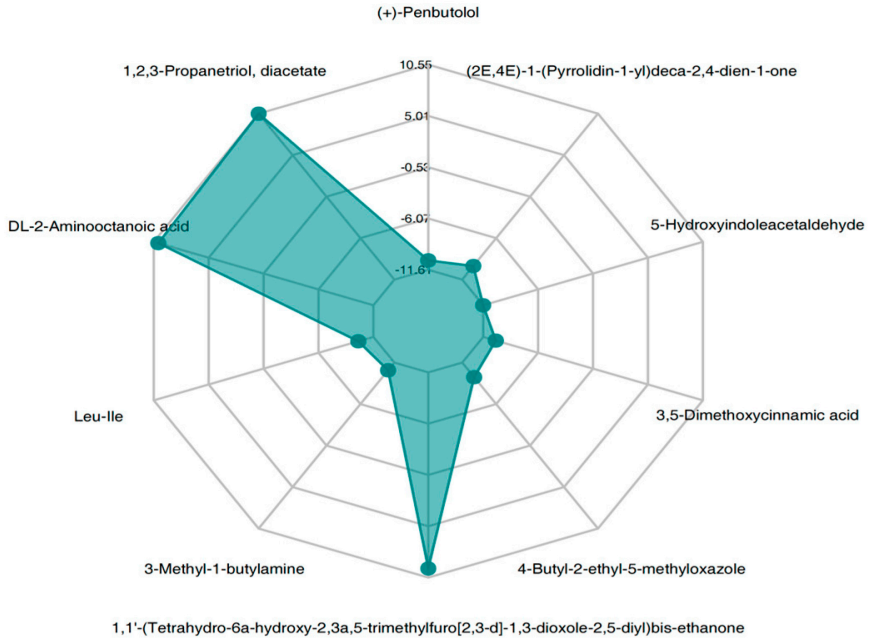
By comparing the non-targeted metabolomics results with the KEGG database, 20 significantly enriched pathways were identified in the Mic3-E1-3d group relative to Control-3d (FDR < 0.05). As shown in Figure 11a, the aminoacyl-tRNA biosynthesis pathway exhibited the highest enrichment (Count = 29, Rich Factor = 5.82). This pathway is a central component in amino acid activation and protein synthesis and is particularly associated with the translation of antimicrobial peptides [40]. The ABC transporter pathway was the next most enriched (Count = 23, Rich Factor = 4.15), with its high expression indicating elevated activity in the transport of transmembrane substances. Microorganisms regulate transport protein functions to optimize their metabolic state, enhancing the excretion of antibacterial metabolites or restricting the intracellular transport of inhibitory substrates, which is a key strategy to adapt to the environment and maximize target metabolite production [41,42]. Notably, the biosynthesis pathway of phenylalanine, tyrosine, and tryptophan ranked fourth (Count = 17, Rich Factor = 3.76). This pathway generates antibacterial precursors, such as benzoic acid and indole acetaldehyde, consistent with the differential metabolites identified, including 2,3-butanedione trimer (Log_2FC = 9.57). DA analysis

based on pathway expression levels (Figure 11b) revealed that aminoacyl-tRNA biosynthesis (DA score = 0.92, $p < 0.001$), ABC transporters (DA score = 0.87), and D-amino acid metabolism (DA score = 0.85) were the most significantly up-regulated pathways. The high activity of the aminoacyl-tRNA pathway directly supports antimicrobial peptide synthesis (e.g., Glycyl-L-leucine, Leu-Ile) by ensuring sufficient amino acid activation and tRNA loading, providing raw materials for peptide chain assembly. Recent studies have confirmed that engineering key components of this pathway, such as aminoacyl-tRNA synthetase, can substantially increase the yield of lipid–peptide antibiotics [42]. Activation of ABC transporters is a common microbial strategy to export antibacterial compounds, with substrates ranging from small phenolic acids to bacteriocin-like peptides [43]. In this study, the increased content of phenolic acid compounds, such as 3,5-Dimethoxycinnamic acid, and their effective interaction with bacterial membranes, is likely attributable to the activity of these transport proteins. Although phenylalanine metabolism (ko00360) did not rank among the top three enriched pathways, its DA score reached 0.81 ($p = 0.003$), further supporting the contribution of the aromatic amino acid metabolism to antibacterial activity.



(a)

Figure 9. *Cont.*



(**b**)

Figure 9. Plot of top 20 differential metabolites ((**a**) Bar Chart, (**b**) Radar Chart). Note: Red indicates an increase, green indicates a decrease, and the size of the dots represents the VIP value.

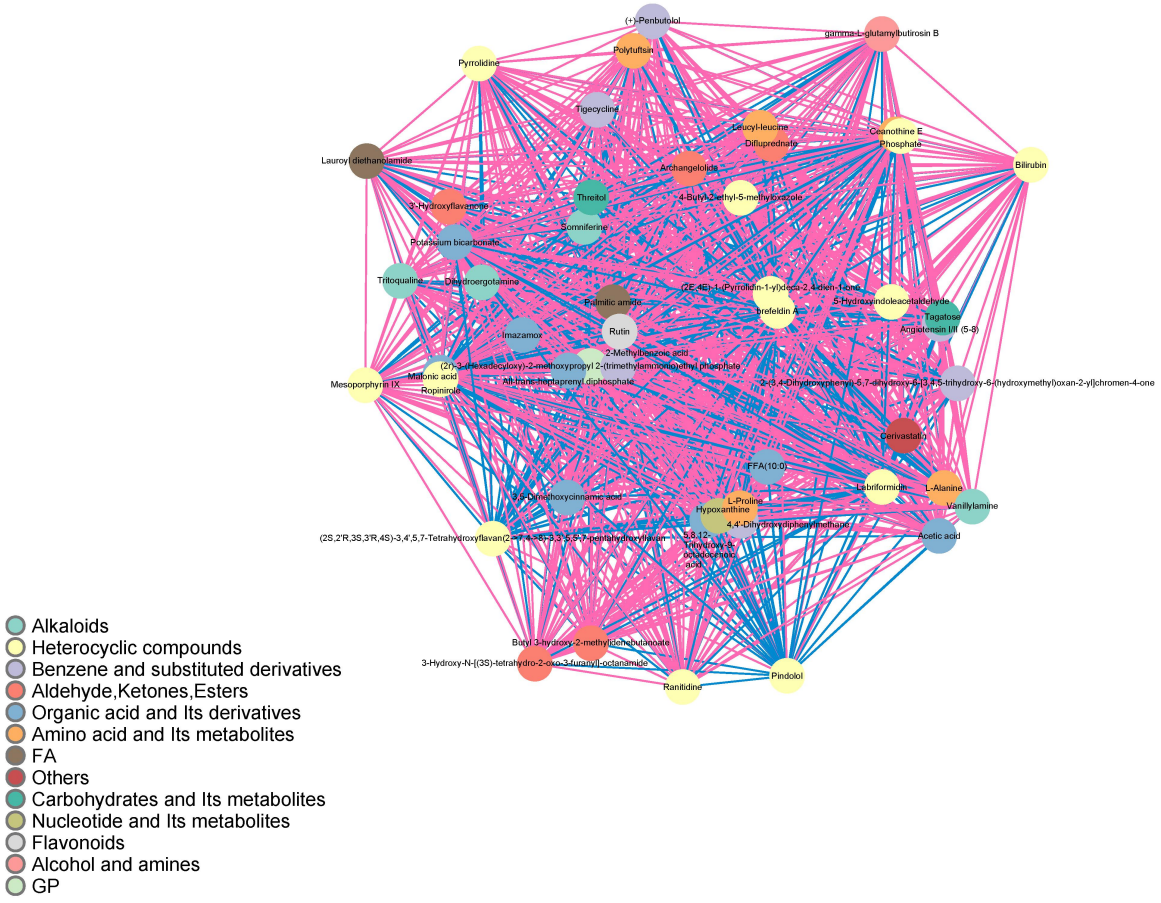


Figure 10. Correlation network regarding differential metabolite categories. Nodes represent metabolite classes, and edges represent strong positive Pearson correlations ($|r| > 0.8$, $p < 0.05$). The network highlights that benzene derivatives and organic acids form a central, highly interconnected cluster, which is strongly linked to other classes such as flavonoids and fatty acids.

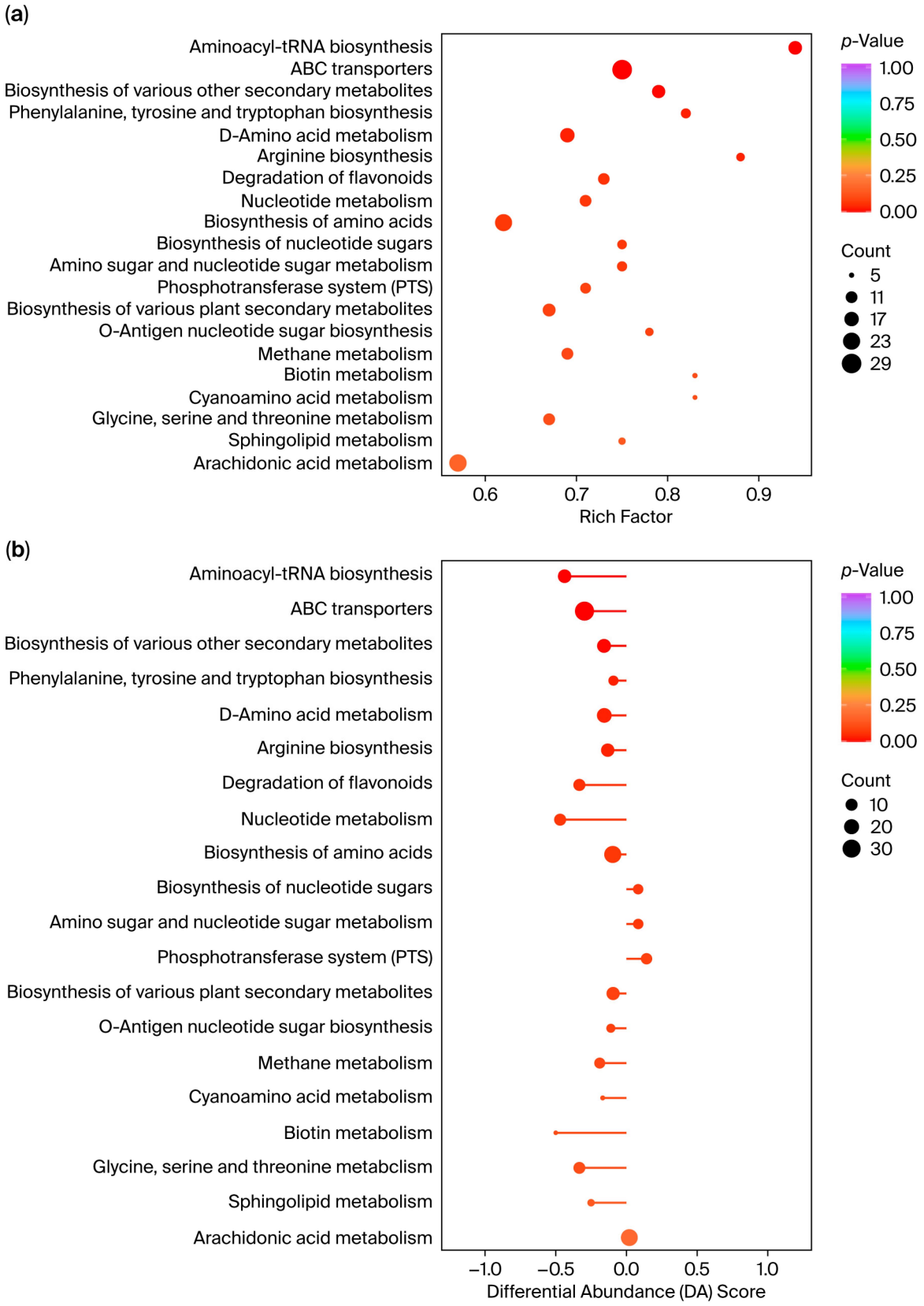


Figure 11. KEGG metabolic pathway diagram. (**a**) KEGG pathway enrichment bubble chart. (**b**) KEGG pathway differential abundance (DA score) analysis chart. The DA score is a quantitative measure (ranging from −1 to 1) representing the coordinated perturbation direction and magnitude of all metabolites within a pathway. A higher positive score indicates a more significant and consistent up-regulation.

4. Discussion

4.1. The Synergistic Antibacterial Mechanism of the Triple Microbiota

Metabolite (Figure S1) correlation analysis revealed that 3,5-Dimethoxycinnamic acid strongly correlated with 5-Hydroxyindoleacetaldehyde (r = 0.82, $p < 0.001$), and both clustered with the B. subtilis marker Leu-Ile. This suggests a metabolic handoff where *B. subtilis* converts fungal-released phenolic acid precursors into indole-type antibacterial compounds. The cascade was initiated by *A. niger*, which secreted hydrolases (e.g., β-glucosidase, PAL) to effectively hydrolyze the plant matrix, thereby releasing amino acid precursors and promoting the accumulation of phenolic acids and flavonoid glycosides [44].

Ultrasonic pre-treatment (160 W, 1 h) of the strains and mixed substrate released antibacterial precursors (e.g., phenylalanine) via enhanced β-glucosidase-mediated lignocellulose hydrolysis [44]. These precursors are converted into phenolic acid intermediates by PAL secreted by *A. niger*, serving as a hub linking primary/phenylpropanoid metabolism and an antibacterial response marker [45], and then utilized by *B. subtilis* to generate membrane-damaging compounds (notably 4-hydroxybenzaldehyde ($Log_2FC = 8.78$) and 2,3-butanedione trimer ($Log_2FC = 9.57$); Section 3.2.3). Notably, PAL activity is induced in *A. niger* enzyme metabolism [46], consistent with its role in initiating the phenolic acid synthesis cascade.

Additionally, aminoacyl-tRNA synthetase specifically activates the tRNA loading of leucine and isoleucine, supplying raw materials for peptide chain elongation in lipopeptides such as surfactin; the efficiency of this process directly determines the final yield of antibacterial lipopeptides. Engineering strategies, such as optimizing aminoacyl-tRNA synthetase function, have been shown to significantly enhance surfactin synthesis [42]. Co-culturing *B. subtilis* with lactic acid bacteria further increases the peptide content [47] and promotes flavonoid release [48]. The significant up-regulation of key antibacterial metabolites identified in this study, such as 2,3-butanedione trimer and 4-hydroxybenzaldehyde (Figure 9a), is consistent with and likely a key contributor to the observed expansion of the antibacterial zone (Figure 2), underscoring the functional synergy within the triple microbiota.

High-yield lipopeptide strains SL-2 and L6 predominantly synthesize surfactin and fengycin, with their crude extracts exhibiting broad antifungal activity. SL-2's enhanced antagonistic spectrum correlates with its enriched genetic repertoire comprising additional secondary metabolic gene clusters and amplified ABC transporter pathways [49]. These traits align with our metabolic findings: the highly active aminoacyl-tRNA pathway (DA score = 0.92, $p < 0.001$) provides activated amino acids for lipopeptide synthesis, while abundant ABC transporters facilitate their export. Together with 4-hydroxybenzaldehyde, they synergistically disrupt bacterial membranes, yielding the observed inhibition zones 17.4 ± 0.8 mm for *E. coli* and 17.7 ± 0.3 mm for *S. aureus*). Given that the primary mechanisms of the identified metabolites (membrane disruption by lipopeptides and phenolic compounds) are effective against a broad spectrum of bacteria and less susceptible to conventional resistance mechanisms, this fermentation strategy holds promise in terms of activity against multidrug-resistant strains. Lipopeptides from *B. subtilis*, such as surfactin and fengycin, have demonstrated efficacy against clinical isolates of methicillin-resistant *S. aureus* [41,48].

The lipopeptide synthesis capability of *B. subtilis* is further supported by strain engineering advances, where NRPS regulation elevated surfactin yield to 10.8 g/L [42]. This aligns with broader metabolic engineering evidence, such as CRISPRi-mediated control of efflux transporters enhancing metabolite export in other systems [50]. Concurrently, the phenylalanine metabolite 4-hydroxybenzaldehyde increased over 430-fold ($Log_2FC = 8.78$). Supporting its role, structural analogs like 4-hydroxyphenylacetic acid have been shown

to disrupt bacterial membrane integrity and potential [51], a mechanism consistent with phenolic-compound-induced oxidative stress [52].

Furthermore, the dramatically upregulated 2,3-butanedione trimer ($Log_2FC = 9.57$) represents another critical aldehyde derivative. The antimicrobial activity of diacetyl-related compounds has been documented against foodborne pathogens [53], while phenolic aldehydes like 4-hydroxybenzaldehyde are known to exert multifaceted effects, including membrane damage [54]. This suggests that both metabolites contribute to the potent antibacterial activity through complex and potentially synergistic mechanisms. This microbial transformation of released precursors, as revealed by LC-MS/MS [37], underpins the synergistic enhancement.

The synergistic effect of *S. cerevisiae* is manifested at the metabolic level: Firstly, *S. cerevisiae*'s inherent ability to synthesize ergosterol significantly enhances the fluidity and stability of the cell membrane, which facilitates robust metabolite transport and sustains microbial activity throughout the fermentation [55]. Secondly, it can markedly increase the extracellular secretion efficiency of antibacterial metabolites, including phenolic acids, flavonoids, and bacteriocins, through its ABC transporter proteins (e.g., homologs of Pdr5p), thereby preventing feedback inhibition and enhancing both the yield and bioavailability of these active compounds [56]. More importantly, *S. cerevisiae* forms functional complementation with *A. niger* and *B. subtilis*: *A. niger* enzymes hydrolyze plant cell walls to release precursor compounds (e.g., pentose derivatives for furan metabolism), *B. subtilis* synthesizes antibacterial peptides and phenolic substances, and *S. cerevisiae*, through sterol-mediated membrane regulation and cooperation with efflux pumps, further enhances the solubility, stability, and efflux of the target metabolites. This mechanism is structurally supported by the endoplasmic reticulum–sterol export site (ERSES), where sterol synthases and transport proteins co-localize and functionally couple at membrane contact sites, providing a cellular basis for efficient, directed metabolite transport [57]. Consequently, *S. cerevisiae* not only acts as a metabolic "boost" to enhance the overall production of antibacterial substances but also enables efficient synergy and functional amplification of the triple microbiota in SSF through membrane biology and transport engineering strategies. While this study demonstrates the potent synergistic effect of the triple microbiota, future work incorporating systematic monoculture fermentation controls will be valuable for precisely delineating the individual contribution of each strain and further optimizing the consortium.

4.2. Considerations on the Limitations of SSF

While this study highlights the efficacy of SSF in enhancing bioactivity, it is important to acknowledge the inherent challenges of this technology. The principal limitation lies in the precise control of physicochemical parameters (e.g., temperature, moisture, pH, and mass transfer), which is more complex than in submerged fermentation. Heterogeneity within the solid substrate can lead to heat accumulation and uneven diffusion of oxygen, nutrients, and metabolites, potentially causing batch-to-batch variation and presenting a bottleneck for scale-up [58,59]. This challenge is also evident in other SSF-based bioprocesses, such as polyhydroxyalkanoate production, where the standardization and scaling of SSF remain underdeveloped compared to SmF [60]. In this work, measures such as incubation in a constant-temperature shaker, periodic manual turning of the substrate, and the use of a fixed initial moisture content were implemented to mitigate these issues. Nevertheless, for robust industrial application, future work must focus on addressing these limitations through advanced online monitoring, process control strategies, and specialized bioreactor designs [58,59]. The development of efficient and scalable bioreactors remains a key research focus for the industrial translation of SSF processes [61].

4.3. Value-Added Potential of Industrialization

This valorization strategy aligns with established industrial models for TCM waste, demonstrating significant economic potential and technical feasibility [62,63]. The scalable "pre-treatment → microbial transformation → product refinement" route underpins a functional upgrade from nutritional improvement to potent antibacterial activity—consistent with the known membrane-disrupting action of *B. subtilis* lipopeptides [64]—and is corroborated by other successful cases, such as the conversion of *Astragalus* residue into functional feed via mixed-microbe fermentation [65]. In this study, the triple microbiota fermented the stems and leaves of *P. sibiricum* and *G. scabra*, increasing antibacterial activity 1.8-fold, further confirming that multi-microorganism synergy can overcome the metabolic bottlenecks of single strains.

From both technical and economic perspectives, the core value of triple microbiota fermentation lies in waste resourcefulness: transforming TCM non-medicinal parts into high-value antibacterial products and mitigating environmental burdens of conventional disposal methods [66]. This consortium strategy builds directly upon foundational successes in single-strain SSF, which has demonstrated the efficacy of microbial fermentation in enhancing bioactivity (e.g., saponins via *A. niger* [67]) and functional properties (e.g., soluble dietary fiber via *B. subtilis* [68]) of agricultural by-products. Beyond antibacterial enhancement, SSF inherently offers advantages in energy consumption and process simplification over traditional extraction methods, strengthening its industrial viability [69,70]. The process integration characteristic of SSF, combined with strategies like optimized reactor loading and gas control, underscores the broader potential for energy-efficient scale-up of the triple microbiota system presented here [71].

5. Conclusions

To address the resource utilization of non-medicinal parts from *Polygonatum sibiricum* and *Gentiana scabra*, a solid-state co-fermentation system employing a triple microbiota (*Aspergillus niger, Bacillus subtilis, Saccharomyces cerevisiae*) was established. This strategy synergistically enhanced antibacterial activity, yielding inhibition zones of 17.4 ± 0.8 mm against *Escherichia coli* and 17.7 ± 0.3 mm against *Staphylococcus aureus*—a 1.8-fold increase over unfermented controls. This enhancement is driven by a core "hydrolysis-synthesis-transport" cascade: *A. niger* hydrolyzes lignocellulose to release precursors; *B. subtilis* synthesizes antimicrobial compounds, supported by significant upregulation of the aminoacyl-tRNA biosynthesis pathway (DA score = 0.92); and *S. cerevisiae* promotes metabolite excretion via ABC transporters. Metabolomics analysis identified 1236 differentially expressed metabolites and pinpointed three key activated pathways: aminoacyl-tRNA biosynthesis, ABC transporters, and phenylalanine-tyrosine-tryptophan biosynthesis, Critical antibacterial metabolites, such as 4-hydroxybenzaldehyde which increased over 400-fold, were significantly accumulated. Consequently, this work provides a scalable, mechanistic-driven strategy for the valorization of traditional Chinese medicine waste into high-value antibacterial products.

Supplementary Materials: The following supporting information can be downloaded at: https://www.mdpi.com/article/10.3390/fermentation11110643/s1. Table S1. Metabolomics data quality assessment metrics. Table S2. Software, parameters, and computational methods for statistical analyses. Figure S1. Pearson heatmap Note: Heatmap of differential metabolite correlations. Rows and columns correspond to metabolite names. Color intensity represents the absolute Pearson correlation coefficient (|r|); red indicates a strong positive correlation, while green indicates a strong negative correlation.

Author Contributions: This research was conceived by C.F., J.F., J.W. and S.M. The manuscript was drafted by C.F. and J.W. Data analysis was conducted by C.F., X.L., M.H. and F.H. Sample collection was carried out by C.F., J.W., W.H., X.L., M.H. and F.H. Research guidance was provided by J.F., W.H. and S.M. J.F. was also responsible for funding acquisition. All authors have read and agreed to the published version of the manuscript.

Funding: This research was supported by the Science and Technology Projects in Liaoning Province [No: 2024JH2/102600213]; the Special Project for Rural Science and Technology in Liaoning Province [No: 2024JH5/10200009]; and the Basic Scientific Research Project of Liaoning Provincial Department of Education Project [No: LJ212413201008].

Institutional Review Board Statement: Not applicable.

Informed Consent Statement: Not applicable.

Data Availability Statement: The original contributions presented in this study are included in the article/Supplementary Materials. Further inquiries can be directed to the corresponding author.

Conflicts of Interest: The authors declare no conflicts of interest.

Abbreviations

The following abbreviations are used in this manuscript:

SSF	Solid-State Fermentation
TCM	Traditional Chinese Medicine
NA	Nutrient Agar
NC	Negative Control
MS	Mass Spectrometry
LC–MS/MS	Liquid Chromatography–Tandem Mass Spectrometry
KNN	K-Nearest Neighbor
CV	Coefficient of Variation
PCA	Principal Component Analysis
UV	Unit Variance
OPLS-DA	Orthogonal Partial Least Squares–Discriminant Analysis
VIP	Variable Importance in Projection
ANOVA	Analysis of Variance
FDR	False Discovery Rate
CLSI	Clinical and Laboratory Standards Institute
KEGG	Kyoto Encyclopedia of Genes and Genomes
CICC	China Center of Industrial Culture Collection
CMCC	National Center for Medical Culture Collections
PDA	Potato Dextrose Agar
LB	Luria–Bertani
YPD	Yeast Extract–Peptone–Dextrose
SD	Standard Deviation
SDF	Soluble Dietary Fiber
FSM	Flaxseed Meal
PAL	Phenylalanine Ammonia-lyase

References

1. Fushun News Network. Talent Nourishes Industries and Writes a New Chapter in Rural Revitalization. 2025. Available online: http://www.fushun.gov.cn/zwgk/002006/002006001/002006001003/20250812/3fc6a390-c57a-4db2-90c8-ab940985b9c3.html (accessed on 14 April 2025).
2. Sun, J.L.; Sun, W.S.; Wang, X.Y.; Zhang, Y.Y. Research Progress on Medicinal Value of *Polygonatum* in Liaoning Province and SWOT Analysis of Its Industrial Development. *Hortic. Seed* **2022**, *42*, 14–17. [CrossRef]

3. Yang, Y. Current Status and High-Quality Development Proposals for Chinese Medicinal Materials Industry in Liaoning Province. *Agric. Sci. Technol. Equip.* **2023**, *4*, 1–4. [CrossRef]
4. Duan, J.A.; Guo, S.; Tang, Z.S.; Wu, Q.N.; Su, S.L.; Wang, M.G.; Yan, H.; Ji, H.; Liu, P.; Zhang, S.; et al. Construction of Circular Utilization Models for Traditional Chinese Medicine Resources and Their Industrial Demonstration. *Jiangsu J. Tradit. Chin. Med.* **2019**, *51*, 1–5.
5. Zhang, X.; Han, X.K.; Liu, X.Y.; Piao, H.L. Study on Development Countermeasures of National Geographical Indication Products of Genuine Medicinal Materials in Liaoning Province. *China Mark.* **2025**, *15*, 17–20. [CrossRef]
6. Li, X.L.; Shi, Y.H.; Hou, C.W.; Liu, Z.X.; Gong, X.J.; Cai, J.L.; Huang, L.; Liu, X.D.; Tong, Q.Z. Current Status and Prospects of Resource Utilization for Non-Medicinal Parts of *Lilium* spp. *Chin. Wild Plant Resour.* **2024**, *43*, 98–104+116.
7. Ji, X.Y.; He, H.J.; Kuang, S.Y.; Liu, Y.F.; Bai, M.; Li, X.M.; Miao, M.S. Modern Research and Comprehensive Application of Non-Medicinal Parts of Chinese Materia Medica in the Pharmacopoeia of the People's Republic of China. *World Chin. Med.* **2024**, *19*, 3650–3654.
8. Chen, H. Preparation of Lignin-Containing Cellulose Nanofibrils and Mechanism Study on Their Property Influences. Ph.D. Dissertation, Nanjing Forestry University, Nanjing, China, 2019. [CrossRef]
9. Huang, C.; Li, Z.X.; Wu, Y.; Huang, Z.Y.; Hu, Y.; Gao, J. Treatment and Bioresources Utilization of Traditional Chinese Medicinal Herb Residues: Recent Technological Advances and Industrial Prospect. *J. Environ. Manag.* **2021**, *299*, 113607. [CrossRef]
10. Fang, Y.Y.; Chen, N.; Xiao, P.; Zhang, S.; Liu, H.F.; Su, S.L.; Guo, S.; Duan, J.A. High-Value Utilization Technology and Approaches of Chinese Medicinal Residues Under the Background of "Dual Carbon". *Chin. J. Chin. Mater. Med.* **2023**, *48*, 5142–5151. [CrossRef]
11. Lyubchyk, S.; Shapovalova, O.; Lygina, O.; Oliveira, M.C.; Appazov, N.; Lyubchyk, A.; Charmier, A.J.; Lyubchik, S.; Pombeiro, A.J.L. Integrated Green Chemical Approach to the Medicinal Plant *Carpobrotus edulis* Processing. *Sci. Rep.* **2019**, *9*, 18171. [CrossRef]
12. Liu, P.L.; Liu, K.L.; Yang, C.X.; Wei, Y.S.; Wang, Y.G. Research and Application Progress in Microbial Fermentation for Improving the Utilization Rate of Plant Meal Resources. *Food Ferment. Ind.* **2025**, *51*, 385–394+405. [CrossRef]
13. Zhao, B.N.; Li, X.; Yang, D.J.; Wan, X.H.; Gao, L.N.; Chu, X.Y.; Sun, X.C.; Liu, Q.Z.; Guo, D.X. Research Progress in the Application of Microbial Fermentation Technology in the Extraction of Plant Active Components. *J. Pharm. Res.* **2025**, *44*, 696–702. [CrossRef]
14. Zhou, L.L.; Wang, Y.H.; Zhang, Y.C.; Zhang, M.L.; Lian, K.Q. Study on the Antibacterial Activity of 4-Terpineol Against *Escherichia coli*. *Chin. Anim. Husb. Vet. Med.* **2025**, *52*, 4497–4504. [CrossRef]
15. Li, Q.; Zhu, X.M. Vanillin and Its Derivatives, Potential Promising Antifungal Agents, Inhibit *Aspergillus flavus* Spores via Destroying the Integrity of Cell Membrane Rather Than Cell Wall. *Grain Oil Sci. Technol.* **2021**, *4*, 54–61. [CrossRef]
16. Chilakamarry, C.C.R.; Mimi Sakinah, A.M.; Zularisam, A.W.; Sirohi, R.; Khilji, I.A.; Ahmad, N.; Pandey, A. Advances in Solid-State Fermentation for Bioconversion of Agricultural Wastes to Value-Added Products: Opportunities and Challenges. *Bioresour. Technol.* **2022**, *343*, 126065. [CrossRef]
17. Izábal Carvajal, A.L.; Sepúlveda, L.; Chávez González, M.L.; Torres León, C.; Aguilar, C.N.; Ascacio Valdés, J.A. Extraction of Bioactive Compounds via Solid-State Fermentation Using *Aspergillus niger* GH1 and *Saccharomyces cerevisiae* from Pomegranate Peel. *Waste* **2023**, *1*, 806–814. [CrossRef]
18. Dai, C.H.; Ma, H.; He, R.H.; Huang, L.R.; Zhu, S.Y.; Ding, Q.Z.; Luo, L. Improvement of Nutritional Value and Bioactivity of Soybean Meal by Solid-State Fermentation with *Bacillus subtilis*. *LWT* **2017**, *86*, 1–7. [CrossRef]
19. Yang, S.Q.; Arslan-Tontul, S.; Fogliano, V.; Casertano, M.; Fan, W.L.; Xu, Y.; Nie, Y.; Vilas-Franquesa, A. Upcycling of Melanoidin-Rich Chinese Distilled Spent Grain through Solid-State Fermentation by *Aspergillus awamori*. *Bioresour. Technol.* **2025**, *416*, 131817. [CrossRef]
20. Li, Q.Y.; Lin, L.B.; Yang, X.J.; Tan, C.Y.; Deng, X.Y. Research Status of Microbial Fermentation of Chinese Herbal Medicines. *Microbiol. China* **2021**, *48*, 2232–2244. [CrossRef]
21. Saldaña Mendoza, S.A.; Palacios Ponce, A.S.; Ruiz, H.A.; Ascacio Valdés, J.A.; Aguilar, C.N. Revalorization of Green Tea Waste through the Production of Cellulases by Solid-State Fermentation Using *Aspergillus niger* 28A. *Biomass Convers. Biorefin.* **2023**, *14*, 16711–16724. [CrossRef]
22. Wen, S.G.; Li, S.; Peng, X.F.; Du, B.Y.; Huang, X.Q.; Qiao, M.W.; Hai, D. Research Progress on Recombinant Expression and Application of Antimicrobial Lipopeptides from *Bacillus subtilis*. *J. Food Saf. Qual.* **2024**, *15*, 105–114. [CrossRef]
23. Lu, Z.; Guo, L.; Chen, X.; Lu, Q.; Wu, Y.; Chen, D.; Wu, R.; Chen, Y. Omics Sequencing of *Saccharomyces cerevisiae* Strain with Improved Capacity for Ethanol Production. *Fermentation* **2023**, *9*, 483. [CrossRef]
24. Maung, T.T.; Gu, B.Y.; Kim, M.H.; Ryu, G.H. Fermentation of Texturized Vegetable Proteins Extruded at Different Moisture Contents: Effect on Physicochemical, Structural, and Microbial Properties. *Food Sci. Biotechnol.* **2020**, *29*, 897–907. [CrossRef] [PubMed]

25. Dorantes-Fuertes, M.-G.; López-Méndez, M.C.; Martínez-Castellanos, G.; Meléndez-Armenta, R.Á.; Jiménez-Martínez, H.-E. Starch Extraction Methods in Tubers and Roots: A Systematic Review. *Agronomy* **2024**, *14*, 865. [CrossRef]
26. Gavrila, A.I.; Vartolomei, A.; Calinescu, I.; Vinatoru, M.; Parvulescu, O.C.; Psenovschi, G.; Chipurici, P.; Trifan, A. Ultrasound-Assisted Alkaline Pretreatment of Biomass to Enhance the Extraction Yield of Valuable Chemicals. *Agronomy* **2024**, *14*, 903. [CrossRef]
27. Marchwicka, M. Influence of pH and Cellic® CTec2 Enzymes Dose on the Glucose Yield after Enzymatic Hydrolysis of Cellulose at 50 °C. *Ann. Wars. Univ. Life Sci. SGGW For. Wood Technol.* **2021**, *114*, 53–58. [CrossRef]
28. de Carvalho Santos Ebinuma, V.; de Oliveira, F.; Veríssimo, N.V.; Pereira, J.F.B.; Pessoa, A. Sterilization in Pharmaceutical Biotechnology. In *Pharmaceutical Biotechnology*; CRC Press: Boca Raton, FL, USA, 2021; pp. 133–145. [CrossRef]
29. Ahamad, M.Z.; Panda, B.P.; Javed, S.; Ali, M. Production of Mevastatin by Solid-State Fermentation Using Wheat Bran as Substrate. *Res. J. Microbiol.* **2006**, *1*, 443–447. [CrossRef]
30. Qin, M.; Guo, L.P.; Pei, L.; He, P.; Zhang, Y.M. Optimization of Optimal Fermentation Process for Traditional Chinese Medicine Residues by Orthogonal Test Method. *Chin. Arch. Tradit. Chin. Med.* **2020**, *38*, 31–34. [CrossRef]
31. Liu, Q.; Luo, G.L.; Guo, L.; Li, X.C.; Song, Z.; Guo, X.L.; Zhong, W. Screening of Fermentation Inoculants for Traditional Chinese Medicine Residues and Optimization of Fermentation Process. *Feed Ind.* **2024**, *45*, 85–94. [CrossRef]
32. Liu, X.Y.; Liao, Y.C.; Wang, Y.; Tian, Q.Y.; Xie, K.X.; Ou, H. Research Progress on the Application of Ultrasonic Combined Technology in the Extraction of Plant Active Ingredients. *Food Ferment. Ind.* **2022**, *48*, 319–327. [CrossRef]
33. Liang, Q.B.; Feng, C.Y.; Xie, Z.R.; Feng, C.Y.; Yuan, W.D.; Chen, C.X.; Wang, X.Y.; Luo, X.J. Consistency Study on Detection of 18 Antibiotic-Resistant Phenotypes in 108 *Escherichia coli* Strains by Kirby-Bauer Method and VITEK2 Method. *J. Food Saf. Qual.* **2024**, *15*, 31–38. [CrossRef]
34. Ibn Awadh, H.; Ahmed, M. In Vitro Antibacterial Activity of Selected Plant Extracts Against *Escherichia coli* and *Staphylococcus aureus* Bacterial Strains. *Discov. Appl. Sci.* **2025**, *7*, 287. [CrossRef]
35. Hettiarachchi, S.S.; Perera, A.Y.P.; Dunuweera, S.P.; Dunuweera, A.N.; Rajapakse, S.; Rajapakse, R.M.G. Comparison of Antibacterial Activity of Nanocurcumin with Bulk Curcumin. *ACS Omega* **2022**, *7*, 46494–46500. [CrossRef]
36. Hassan, Z.; Fischbach, N.; Hofsommer, M.; Slatnar, A. Development and Validation of HPLC-MS/MS Method for Simultaneous Analysis of B Vitamins Present Naturally or After Fortification in Fruit Juices. *LWT* **2023**, *184*, 115103. [CrossRef]
37. Yu, X.; Cheng, H.; Chen, Y.L.; Ho, C.-T.; Wu, X.; Huang, Y.X.; Gao, Y.; Hou, A.X.; Li, Z.J.; Wang, Y.L.; et al. UPLC–QQQ–MS/MS-Based Widely Targeted Metabolomic Analysis Reveals the Effect of Solid-State Fermentation with *Eurotium cristatum* on the Dynamic Changes in the Metabolite Profile of Dark Tea. *Food Chem.* **2022**, *378*, 131999. [CrossRef]
38. *M07-A10*; Methods for Dilution Antimicrobial Susceptibility Tests for Bacteria That Grow Aerobically; Approved Standard—Tenth Edition. Clinical and Laboratory Standards Institute: Wayne, PA, USA, 2015.
39. Kauffmann, A.C.; Castro, V.S. Phenolic Compounds in Bacterial Inactivation: A Perspective from Brazil. *Antibiotics* **2023**, *12*, 645. [CrossRef] [PubMed]
40. Major, D.; Flanzbaum, L.; Lussier, L.; Davies, C.; Caldo, K.M.P.; Acedo, J.Z. Transporter Protein-Guided Genome Mining for Head-to-Tail Cyclized Bacteriocins. *Molecules* **2021**, *26*, 7218. [CrossRef]
41. Su, Y. Functional Identification of Purine Transporters in Bacillus subtilis and Their Application in Riboflavin Metabolic Engineering Modification. Master's Thesis, Tianjin University of Science and Technology, Tianjin, China, 2021. [CrossRef]
42. Hermann, A.; Hiller, E.; Hubel, P.; Biermann, L.; Perino, E.H.B.; Kuipers, O.P.; Hausmann, R.; Lilge, L. Genetic Code Expansion for Controlled Surfactin Production in a High Cell-Density Bacillus subtilis Strain. *Microorganisms* **2025**, *13*, 353. [CrossRef]
43. Beis, K.; Rebuffat, S. Multifaceted ABC Transporters Associated to Microcin and Bacteriocin Export. *Res. Microbiol.* **2019**, *170*, 399–406. [CrossRef]
44. Mamy, D.; Boateng, I.D.; Chen, X.M. Ultrasound-Assisted Solid-State Fermentation by *Aspergillus niger* Increased Phenolics and Antioxidants' Accumulation in *Citrus reticulata* Peels. *Food Biosci.* **2025**, *63*, 105699. [CrossRef]
45. Dhanabalan, S.; Muthusamy, K.; Iruthayasamy, J.; Kumaresan, P.V.; Ravikumar, C.; Kandasamy, R.; Natesan, S.; Periyannan, S. Unleashing Bacillus Species as Versatile Antagonists: Harnessing the Biocontrol Potentials of the Plant Growth-Promoting Rhizobacteria to Combat *Macrophomina phaseolina* Infection in Gloriosa superba. *Microbiol. Res.* **2024**, *283*, 127678. [CrossRef]
46. Dong, X.X. Analysis of Effects and Mechanism of ARTP Mutagenesis on the Metabolism of Tannase from *Aspergillus carbonarius*. Master's Thesis, Nanchang University, Nanchang, China, 2021. [CrossRef]
47. Ezekiel, O.O.; Oguntoye, M.A.; Salami, N.O. Solid-State Fermentation with Bacillus subtilis Co-Cultured with Probiotic *Lactobacillus* spp. Enhances the Bioactive Peptides, Nutritional and Antioxidative Potentials of Tamarind Seed. *Biocatal. Agric. Biotechnol.* **2024**, *48*, 103368. [CrossRef]
48. Liu, Y. Dual-Bacterial Fermentation of Oats Improves Polyphenol Antioxidant Activity and Its In Vitro Digestion Characteristics. Master's Thesis, South China University of Technology, Guangzhou, China, 2019. [CrossRef]

49. Bai, X.; Yi, L.; Zhao, S.; Xiu, J.; Li, P.; Shi, R.; Liang, X.; Zhang, Y. Identification and Comparative Genomic Analysis of Two *Bacillus subtilis* Producing Antifungal Lipopeptide. *Pestic. Biochem. Physiol.* **2025**, *213*, 106470. [CrossRef]
50. Gao, Z.Q. Screening and Application of L-Histidine Transporters in *Escherichia coli*. Master's Thesis, Tianjin University of Science and Technology, Tianjin, China, 2024. [CrossRef]
51. Liu, Y.J.; Shi, C.H.; Zhang, G.L.; Zhan, H.L.; Liu, B.N.; Li, C.; Wang, L.; Wang, H.; Wang, J.H. Antimicrobial Mechanism of 4-Hydroxyphenylacetic Acid on Listeria monocytogenes Membrane and Virulence. *Biochem. Biophys. Res. Commun.* **2021**, *572*, 145–150. [CrossRef]
52. Arunachalam, K.; Ravi, J.; Tian, X.R.; Shunmugiah, K.P.; Shanmugaraj, G.; Shi, C.L. Antibacterial Activity of 2-Hydroxy-4-Methoxybenzaldehyde and Its Possible Mechanism Against *Staphylococcus aureus*. *J. Appl. Microbiol.* **2023**, *134*, lxad144. [CrossRef]
53. Xiang, Q.S.; Ma, Y.F.; Shen, R.L. Research Progress on Formation Mechanisms and Detection Methods of 2,3-Butanedione in Foods. *Food Ferment. Ind.* **2014**, *40*, 208–214. [CrossRef]
54. Qian, L.; Zhu, X.M.; Xie, Y.L.; Ren, S.L. 2-Hydroxy-4-methoxybenzaldehyde Inhibits the Growth of *Aspergillus flavus* via Damaging Cell Wall, Cell Membrane, Manipulating Respiration Thus Creating a Promising Antifungal Effect on Corn Kernels. *Int. J. Food Sci. Technol.* **2021**, *56*, 178–184. [CrossRef]
55. Ke, X.; Shen, Y.; Cao, L.S.; Zhang, B.; Liu, Z.Q. Reinforcement of Sterols Production Through Directed Storage and Transportation in Yeast: A Review. *Chin. J. Biotech.* **2021**, *37*, 3975–3987. [CrossRef]
56. de Moraes, D.C.; Tessis, A.C.; Rollin-Pinheiro, R.; Princival, J.L.; Villar, J.A.F.P.; Barbosa, L.A.; Barreto-Bergter, E.; Ferreira-Pereira, A. Digoxin Derivatives Sensitize a *Saccharomyces cerevisiae* Mutant Strain to Fluconazole by Inhibiting Pdr5p. *J. Fungi* **2022**, *8*, 769. [CrossRef]
57. Encinar del Dedo, J.; Fernández-Golbano, I.M.; Pastor, L.; Meler, P.; Ferrer-Orta, C.; Rebollo, E.; Geli, M.I. Coupled Sterol Synthesis and Transport Machineries at ER–Endocytic Contact Sites. *J. Cell Biol.* **2021**, *220*, e202010016. [CrossRef]
58. Qiu, Y.X.; Liu, Y.Y.; Chen, S.X.; Fang, C.; Zhang, R.Q.; Zhang, M.X. Analysis of Heat and Mass Transfer Behaviors in the Enzyme-Producing Reaction System of Solid-State Fermentation. *Prog. New Energy* **2022**, *10*, 463–470.
59. Catalán, E.; Sánchez, A. Solid-State Fermentation (SSF) versus Submerged Fermentation (SmF) for the Recovery of Cellulases from Coffee Husks: A Life Cycle Assessment (LCA) Based Comparison. *Energies* **2020**, *13*, 2685. [CrossRef]
60. Piecha, C.R.; Alves, T.C.; Zanini, M.L.O.; Corrêa, C.P.L.; Leite, F.P.L.; Galli, V.; Diaz, P.S. Application of the Solid-State Fermentation Process and Its Variations in PHA Production: A Review. *Arch. Microbiol.* **2022**, *205*, 11. [CrossRef]
61. Leite, P.; Sousa, D.; Fernandes, H.; Ferreira, M.; Costa, A.R.; Filipe, D.; Gonçalves, M.; Peres, H.; Belo, I.; Salgado, J.M. Recent Advances in Production of Lignocellulolytic Enzymes by Solid-State Fermentation of Agro-Industrial Wastes. *Curr. Opin. Green Sustain. Chem.* **2021**, *27*, 100407. [CrossRef]
62. Duan, J.A.; Tang, Z.S.; Wu, Q.N.; Su, S.L.; Guo, S.; Yan, H.; Qian, D.W. Establishment and Promotion Application of a Suitable Technology System for Circular Utilization in the Industrialization Process of Traditional Chinese Medicine Resources. *Chin. J. Mod. Chin. Med.* **2019**, *21*, 20–28. [CrossRef]
63. Duan, J.A.; Guo, S.; Su, S.L.; Guo, L.P.; Zhao, M.; Liu, R.; Yan, H.; Wang, T.J.; Wang, Z.Z.; Xiao, W.; et al. Innovation and Practice of Traditional Chinese Medicine (TCM) Resource Chemistry Discipline Leading the Whole-Industry-Chain Circular Utilization and Green Development of TCM Resources. *J. Nanjing Univ. Tradit. Chin. Med.* **2024**, *40*, 1114–1122. [CrossRef]
64. Filipe, D.; Vieira, L.; Ferreira, M.; Oliva-Teles, A.; Salgado, J.; Belo, I.; Peres, H. Enrichment of a Plant Feedstuff Mixture's Nutritional Value through Solid-State Fermentation. *Animals* **2023**, *13*, 2883. [CrossRef]
65. Xie, Y.J.; Shen, K.X.; Yan, K.X.; Li, H.W.; Liu, H.F.; Yang, R.Q.; Guo, S.; Duan, J.A. Experimental Study on Production of Functional Feed from *Astragalus membranaceus* Residue by Mixed-Strain Solid-State Fermentation. *Feed Ind.* **2024**, *45*, 83–93. [CrossRef]
66. Hasan, M.R.; Anzar, N.; Sharma, P.; Malode, S.J.; Shetti, N.P.; Narang, J.; Kakarla, R.R. Converting Biowaste into Sustainable Bioenergy Through Various Processes. *Bioresour. Technol. Rep.* **2023**, *23*, 101542. [CrossRef]
67. Yao, R.J. Resource Utilization and Biotransformation of *Panax japonicus* C.A. Meyer and Its Pharmacodynamic Study on Alleviating Chronic Kidney Disease (CKD). Master's Thesis, Chengdu University, Chengdu, China, 2025. [CrossRef]
68. Hou, C.P.; Zhang, Y.Y.; Chen, J.X.; Hu, J.G.; Yang, C.X.; Chen, F.S.; Zhu, T.W.; Xin, Y.; Geng, X.H. Optimization of Solid-State Fermentation Process for Dietary Fiber in Flaxseed Meal and Analysis of Its Microstructure and Functional Properties. *Foods* **2025**, *14*, 1722. [CrossRef] [PubMed]
69. Liu, Y. Study on Physicochemical Properties of Solid-State Fermentation Medium and Novel Solid-State Fermentation Processes. Ph.D. Dissertation, University of Chinese Academy of Sciences (Institute of Process Engineering, Chinese Academy of Sciences), Beijing, China, 2019. Available online: https://kns.cnki.net/kcms2/article/abstract?v=lH-stw_WZ3fZBEXehapy4xRqjdtU9QJFJus9BS-ONgaWSrvbzPbcnJIzvpnFVXF0EU3SXV6CkzaOD89upJ0RqxlI-fqUY7hQ4kC2ofgnqxB1hvxeVJIfsnSNSZiYZe_mZiVBCU3eTJgjpiVnSwpKn4pzSbJWW55BFoZ7reo3so9KVZ-HjtgbpN8AFKLuSC5w&uniplatform=NZKPT&language=CHS (accessed on 12 September 2025).

70. Zhou, J.Z.; Feng, J.X.; Xu, Q.; Zhao, Y.J. A Much Cheaper Method to Separate Ethanol After Solid-State Fermentation Process in Renewable Energy Production. *Renew. Energy* **2018**, *123*, 675–682. [CrossRef]
71. Chang, S.Y.; Yun, C.K.; Yang, B.Q.; Duan, J.N.; Chen, T.Y.; Liu, L.; Li, B.F.; Guo, S.; Zhang, S. Comprehensive Reutilization of *Glycyrrhiza uralensis* Residue by Extrusion-Biological Pretreatment for Coproduction of Flavonoids, Cellulase, and Ethanol. *Bioresour. Technol.* **2024**, *406*, 131002. [CrossRef] [PubMed]

Disclaimer/Publisher's Note: The statements, opinions and data contained in all publications are solely those of the individual author(s) and contributor(s) and not of MDPI and/or the editor(s). MDPI and/or the editor(s) disclaim responsibility for any injury to people or property resulting from any ideas, methods, instructions or products referred to in the content.